Study of Waveguide and Anisotropy Effects upon Surface Acoustic Wave Velocities in Thin Films

by

Ariya Akthakul

BS. Chemical Science and Engineering, Kobe University

Submitted to the Department of Materials Science and Engineering in partial fulfillment of the requirements for the degree of

Master of Science in Materials Science and Engineering

at the

MASSACHUSETTS INSTITUTE OF TECHNOLOGY

June 1998

Author .....
Department of Materials Science and Engineering
May 8, 1998

Certified by ...
Keith A. Nelson, Professor of Chemistry
Department of Chemistry
Thesis Supervisor

Certified by .....
David Roylance, Associate Professor of Materials Engineering
Department of Materials Science and Engineering
Thesis Reader

Accepted by .....
Linn Hobbs, John F. Elliot Professor of Materials
Chairman, Department Committee on Graduate Students
Department of Materials Science and Engineering

Studies of Waveguide and Anisotropy Effects upon Surface Acoustic Wave Velocities in Thin Films

by

Ariya Akthakul

Submitted to the Department of Materials Science and Engineering
on May 8, 1998, in partial fulfillment of the requirements for the
degree of Master of Science in Materials Science and Engineering

Abstract

Impulsive Stimulated Thermal Scattering (ISTS) is an *in-situ* non-destructive characterization technique based on laser excitation and detection of surface acoustic waves (SAWs) for mechanical properties of thin metal films in the microelectronic industry. In this work, the effect of elastic anisotropy from silicon wafers on ISTS measurements has been studied. It has been shown that for films of submicron thickness, the anisotropic effects on acoustic velocities are substantial. Moreover, at a particular orientation of propagating SAWs, two surface acoustic modes are observed rather than only one acoustic mode as in an isotropic model. With regard to dispersive behavior, a previously unknown result has been established that the pseudo-surface wave branch of an uncoated substrate is a $qd->0$ limit for the second-order acoustic waveguide mode of a film-substrate system. Theoretical analysis for calculating acoustic modes of a supported film for arbitrary orientation, along with an experimental technique featuring optically heterodyned signal detection, provide an adequate basis for accurate characterization of thickness and elastic properties of thin films on anisotropic substrates. Furthermore, in the preliminary study of the waveguide effect on Damascene Structure, it has been considered that the widths of the bar structures as well as the spaces between the bar structures should be included in the scaling parameters for dispersion curves.

Thesis Supervisor: Keith A. Nelson
Thesis Reader: David Roylance

Table of Content

List of Figures

Acknowledgments

First of all, I would like to express my gratitude to my advisor Keith Nelson for his kindness and great advice. Keith introduced me laser spectroscopy in studying acoustics. He guided me through the world of science and always gave me simple, yet meaningful and profound explanations. Another person that I greatly appreciate especially for his patience and generosity is Dr. Alex Maznev. I developed my experimental skills along with my approaches to scientific reasoning thanks to his presence and attention. Without him, I would have been lost in the cloud of ignorance. I would like to thank Randy Logan for his important guidance during the early period of my study in addition to all the members in the Nelson Group for their support and conversations. Also, I would like to mention Active Impulse Systems, Inc. for the Damascene experiments, especially Dr. Matt Banet for his discussion and hospitality. Thanks to all my friends who gave me support and helped me through all the difficulties. Special thanks to Kung and Tengo for always being with me. Finally, I would like to thank my family for their huge support that always comforts me.

Chapter 1: Introduction

Due to the rapid growth of the electronics industry, nanotechnology has been extensively developed, especially in the area of thin-film materials. The coating of films for the purpose of promoting material properties such as electric or thermal conductivity, strength and toughness to operating environments, as well as for the purpose of oxidation or diffusion control exemplifies the broad range of thin-film applications. In general, the performance of thin-film materials depends upon physical, mechanical and thermal properties of the film-substrate system. In order to maintain superior performance during the operation time, it is important that thin-film materials maintain strong integrity; therefore, characterization techniques to ensure performance reliability become a significant demand for practical applications. Issues of reliability have become highly critical with the increasing degree of miniaturization in integrated circuit fabrication, which generally uses thin metal films on a single crystal silicon wafer as diffusion barriers, adhesion promoters, or conductors.

Various evaluation techniques have been developed; some methods are destructive, some are non-destructive. In general, standard tests to obtain information on tensile, compressive, shear and impact properties of materials are destructive. In fact, it is considered more favorable to obtain information on material properties under operating conditions which are non-destructive. Non-destructive techniques can be classified into two categories: active and passive. Passive techniques usually involve the assessment of sample quality through some responses during either a typical load environment or a proof cycle. The techniques include acoustic emission, noise analysis, leak testing, visual examination, and some residual magnetic techniques. On the other hand, active techniques analyze responses from the sample after a disturbance has been introduced into or onto the sample.

Magnetic particle, ultrasonics testing, Eddy currents, and radiography methods are among the typical active techniques[1]. All these non-destructive testing methods may be used independently or in conjunction with one another to perform the inspection, depending on the type of applications.

Non-destructive testing is of great importance to ensure the performance of thin-film material components. With non-destructive methods, the reliability on functional design is provided in addition to the reduction in frequency of unscheduled maintenance[2]. Among various non-destructive characterization techniques for the physical and mechanical properties of thin-film materials, testing methods using acoustic waves are widely studied because of their versatile applicability to most materials. Compared to some other non-destructive methods such as TEM and SEM which pose limitations on the sample dimension and evaluation condition, launching acoustic waves and detecting the signal provides us more flexibility to gain information on mechanical properties, surface flaws or surface inhomogeneity[3]. In contrast with electromagnetic waves, where there are only pure transverse modes, acoustic waves have mechanical spectra that include both compressional and transverse waves. The availability of both modes is considered an advantage because it permits separation or sorting out of effects which interact differently with the two types of wave.

In general, the acoustic waves produce small-amplitude mechanical vibrations and induce both longitudinal and shear stresses in the solid. Information on the structural properties of a substance can be obtained by measuring both the velocity and the attenuation of an acoustic wave. The attenuation of an acoustic wave is associated with absorption of elastic waves and the scattering of elastic waves by structural inhomogeneities. The former is due to internal friction that causes the conversion of elastic into thermal energy resulting in the elastic energy lost by scattered fields, which is gradually absorbed in the

material. However, the latter may be the dominant attenuation mechanism in polycrystalline, composite, and ceramic materials[4-5].

The phase velocity of the acoustic wave depends on the elastic constants, thickness and density of thin-film materials. As it is known that the anisotropy effect, which is the orientation-dependence of physical and mechanical properties, should be observed in most materials, the resulting acoustic probe would vary along different orientations. In an *isotropic* material, which has only two independent elastic moduli, there exist two kinds of elastic waves: the longitudinal and the shear. In an *anisotropic* material, three kinds of bulk elastic waves may propagate: a quasi-longitudinal and two quasi-transverse waves, differing in polarizations and velocities. To determine the set of elastic constants, one must measure the phase velocities in several different orientations relative to the crystallographic axes.

Mechanical properties of the film-substrate system are controlled by both the bulk properties of the film and substrate along with the properties of the film-substrate interface like the adhesion of the film-substrate. According to *Rayleigh*[6], an elastic surface wave may propagate along the surface of a body. The elastic energy of the surface wave decays nearly exponentially from the surface and is localized in the subsurface layer with a thickness of the order of the acoustic wavelength λ. Below this depth, there is virtually no transport of elastic energy. For a surface acoustic wave in a layered structure, there is typically a wide range of several modes of wave propagation and all the modes in this system are dispersive, i.e. velocities depend on the wave vectors in each mode[7].

Furthermore, the presence of a thin film on a substrate surface changes the effective surface stiffness, and thus affects the acoustic velocity. In general, there are two types of loading conditions that may cause variations in the acoustic velocities of film-substrate systems. A film loading case is represented when the stiffness of the film is greater than

that of the substrate, resulting in the dependence of acoustic velocities on the wavevector toward higher values compared to the acoustic velocities on the substrate alone. In contrast, a substrate loading case is considered when the stiffness of the film is smaller than that of the substrate, resulting in a waveguide effect to lower acoustic velocities in the system. Silicon in particular, as a major substrate in the current electronics industry, is known to be anisotropic with high stiffness; hence, the film systems in most electronic applications tend to display the substrate loading case. A film whose thickness is much less than an acoustic wavelength is subjected to a compression-tension strain in the course of surface-wave propagation. The strain arising in the film is similar to the strain in a thin plate upon propagation of a longitudinal plate mode[5]. Measurements of the surface-wave velocities can also yield information on the adhesive degree and the condition of the bond between the film and the substrate[8].

Many researchers have studied anisotropy in surface acoustic waves (SAWs). The problems of SAW propagation in an anisotropic crystal cannot be solved analytically except for the case of symmetric cuts and directions in cubic and hexagonal crystals[9]. *Farnell*[10] developed a numerical method and calculated the angular dependence of the acoustic velocity propagating along several crystallographic planes of cubic crystals. Several reports compare experimental measurements of surface waves by different techniques to the theoretical values[11-12]. However, the behavior of acoustic waves on more complicated systems such as in isotropic layers on anisotropic substrate systems remains not fully understood.

This thesis studies an *in-situ* and non-destructive ultrasonic technique using a laser-induced thermal grating method called Impulsive Stimulated Thermal Scattering (ISTS). ISTS is a technique which is practical for surface acoustic velocity measurements

and the study of elastic and thermal properties in the bulk and surface of materials which may be used for feedback and *in-situ* control over thin-film fabrication and curing.[13-14].

An ISTS experiment is comprised of two parts: crossed excitation laser pulses and a probe laser pulse. The crossing of excitation laser pulses generates a thermal grating pattern onto the surface which launches the acoustic waves to propagate along the surface. Then, the acoustic waves induce material motions at and near the surface, resulting in surface ripple displacements. These surface ripples act as a transient grating and diffract the incoming probe laser pulse. The first-order diffraction signal is directed to the detector for a determination of acoustic velocity and further of the mechanical properties of thin-film materials.

In ISTS, from the photothermal and photoacoustic responses, physical and mechanical properties of thin film systems can be determined by fitting the acoustic velocity dispersion curves scaled with the product of wavevector and film thickness. It is expected that the angular dependence of acoustic velocities should also be observed in ISTS measurements. Measuring the anisotropy effect in acoustic wave velocity along the surface enables us to determine physical and mechanical properties of the system with a higher accuracy compared to the isotropic model that is currently used[6]. Here our measurement regime is restricted to only the velocities of the first and second waveguide modes. The dispersive behavior calculated theoretically suggests the coupling effect of the Love-type wave and the Rayleigh-type wave in these two modes.

In previous ISTS experiments, *Rogers et al*[14] fitted the data with a depth-independent isotropic model. They concluded that the shifts of waveguide frequencies due to non-idealities in this system were within the experimental uncertainty. The main source of error was in the mechanical measurement of the scattering angles to determine the wavevectors. However, the effect of anisotropy also has to be taken into account in order

to enhance the accuracy and reliability of the ISTS technique. Hence, in this thesis we seek to explore the effect of anisotropy on phase velocities of the surface waves measured by ISTS techniques, and to understand SAWs as studied in layered structures on anisotropic substrates.

Furthermore, apart from the practical applications, the study of the anisotropy effect itself is very interesting, particularly since the formulation of acoustic modes from thin supported films by *Farnell and Adler*[15] does not quite relate the Leaky waves to Rayleigh and Love-type wave modes. Therefore, this thesis will discuss the relationship between pseudo-surface waves and the waveguide modes.

Chapter 2: Background and Theory

2.1 Surface Acoustic Waves in Solids

2.1.1 Rayleigh Waves

A Rayleigh wave is a typical surface wave near a free boundary whose amplitude decreases exponentially with distance from the surface. It propagates slightly more slowly than a shear wave. The Rayleigh wave velocity v_R is independent of frequency ($q=\omega/v_R$). In other words, the Rayleigh waves in classical elastic bodies are dispersionless, and the ratio v_R/c_t is defined by the ratio of the longitudinal velocity to the transverse velocity (c_l/c_t) which depends only on Poissons ratio σ. The displacement of particles consists of elliptical motions and the particles on the wave crests move in the direction opposite to the direction of the wave propagation as shown in Fig.[1].

2.2 Surface Waves in Anisotropic Materials

It has been argued that a surface wave can propagate along any cut of a given crystal in any arbitrary direction[16-18]. The Lothe-Barnett theorem stated that a Rayleigh wave always exists except for the cases when a bulk wave with lower velocity satisfies the boundary conditions for a surface skimming wave. In piezoelectrics, such waves often become the Gulyaev-Bleustein waves. And a non-piezoactive Rayleigh wave can also propagate in the same direction[19].

As a rule, one can always find at least one solution corresponding to a surface wave. Again, since one side is free, the velocity of this surface wave is less than the velocities of bulk waves which can propagate in material along the same direction. At first, we shall start with the expression for displacements of the surface waves that satisfy the boundary conditions[11]. We shall notice later that the obtained solution is often like a Rayleigh wave in isotropic materials with the displacements lying in the sagittal plane or slightly deflected from it. Another study of the surface wave problem in anisotropic solids by using a surface Green function matching analysis also yielded similar results[18].

2.3 The Wave Equation and Surface Wave

If the body forces and piezoelectric effects are negligible, the wave equation can be written in the form:

$$\rho \frac{\partial^2}{\partial t^2} uj = Cijkl \frac{\partial^2}{\partial x_i \partial x_l} uk \qquad (1)$$

for $i,j,k,l = 1,2,3$ where the u_i are the displacement components along the Cartesian axes x_i to which stiffness tensor c_{ijkl} is referred. ρ is the density of the medium. In the bulk wave problem, the simplest solution will be in the form

$$u = A \exp[ik(l_1 x_1 + l_2 x_2 + l_3 x_3 - vt)] \qquad (2)$$

resulting in three displacement vectors; one quasi-longitudinal and the other two quasi-transverse.

For the surface wave problem, the solutions of the wave equation should be decaying with depth below the surface in the form

$$u = \alpha \exp[ikl_3 x_3] \exp[ik(l_1 x_1 + l_2 x_2 - vt)] \tag{3}$$

Here we take x_3 as the outward normal to the traction-free surface of the medium. Now, the x_3 component of the displacement is to be considered as the amplitude term of the solution leaving just x_1 and x_2 to describe wave propagation. This form of displacement will be such that the amplitudes of all the displacements will vanish as the depth approaches infinity (x -> - *infinity*). The propagation vector is assumed to be parallel to the surface even though there may be a real part in l_3.

The formulation of the surface wave problem will be that for a set propagation direction along the surface (l_1,l_2). We plug the displacement equation into the wave function resulting in the secular equation in the surface-wave case. This secular equation is a sextic equation of l_3 with phase velocity v as a parameter, and thus gives a relationship between the unknown l_3 and v. The boundary conditions enforce the continuity of the longitudinal and vertical particle displacements, the sagittal shear stress, and the vertical compressional stress at all material interfaces and the vanishing of the sagittal shear stress and vertical compressional stress at all free surfaces. The velocities of the waveguide modes are calculated by iterative search for the zeros of the determinant determined by the system of equations generated by the boundary conditions of equations. Finally, there are three lower-half-plane roots to the secular equation that give the propagating terms on the

semi-infinite surface. The final solution for the surface wave that satisfies the surface conditions at infinite depth is

$$u_i = \left(\sum_{n=1}^{3} C_n \alpha_i^{(n)} \left(\exp[ik(l_1 x_1 + l_2 x_2 + l_3^{(n)} x_3 - vt)]\right)\right) \tag{4}$$

C_n are the weighing factors determined by satisfying the traction-free boundary conditions. Hence, for general orientation of the free surface with respect to the crystallographic axes, there will be whole angular ranges of directions in which the surface waves may be propagated and not just the discrete directions as suggested by Synge[20].

2.3.1 General Isotropy

In an isotropic solid, the solutions for propagation of SAWs are greatly simplified by the stiffness tensor of the isotropic solid itself. There are two solutions of waves propagating along the traction-free surface corresponding to this case. First, there is a pure-mode Love wave or a transverse bulk wave with particle displacement parallel to the surface and with amplitude constant as a function of depth beneath from the surface. Second, there is a surface wave solved by the iterative search with velocity as a function of c_{11} and c_{12}. The wave creates elliptical particle displacements at any depth which vanish at infinite depth. The plane of the ellipse is in the sagittal plane with the major axis perpendicular to the free surface. The shape of the ellipse changes with depth. This is called a pure-mode Rayleigh wave.

2.3.2 General Anisotropy

In contrast with the acoustic wave in an isotropic solid, a dependence of the surface acoustic phase velocity on the direction of wave propagation is expected. When the wave equation is solved and the surface boundary condition is considered, the solutions are not always pure-mode Rayleigh and Love waves and there will be an introduction of real parts of the roots of the sextic equation of l_3 which indicates the change of the amplitudes of particle displacement with depth in an exponential damped sinusoidal way. Indeed, the introduction of the real part of l_3 also shows a degree of propagation vector tilt away from the surface.

Here, we consider the anisotropy ratio

$$\eta = \frac{2c_{44}}{(c_{11} - c_{12})} \tag{5}$$

This is a magnitude of anisotropy indicating the ratio of the stiffness along the axis and across the axis compared to the isotropic case ($\eta = 1$).

For acoustic waves propagating on an anisotropic traction-free solid surface, there are also two types of waves. First, there is the transverse bulk shear wave or Love-type wave with the particle displacement along the surface which satisfies the traction-free boundary condition but whose amplitudes do not decay with depth. Second, there is the surface wave or Rayleigh-type wave whose solution could be found by a general search procedure.

In a particular propagation direction, the surface wave solution displays certain common characteristics. It has pure-mode Rayleigh-type solutions, the solutions that have only two rapidly damped terms of particle displacements which also only lie in the sagittal plane, have a principal axis of the surface-displacement ellipse perpendicular to the free surface, and having the power-flux collinear with the propagation vector.

Another notation about the solution of the acoustic wave is the Leaky type solution or pseudo-surface wave. It is a Rayleigh-type wave which has a phase velocity higher than that of the lowest transverse bulk wave. These types of solution can also be observed in some set of circumstances. It has been called "pseudo" or "leaky" since there is a small third term in the solutions that indicates a quasi-transverse bulk wave with its propagation vector in the sagittal plane but tilted down into the solid which carried energy away from the surface, yet does not satisfy the conditions of surface wave. However, for many cases the radiating term is small enough that the waves satisfy most of the experimental conditions for surface waves and thus are observable.

2.4 Pseudo-surface Waves

On the anisotropic free surface, a particular mode of elastic surface wave propagation may exist. This mode has a phase velocity that exceeds that of the lowest quasitransverse bulk wave in the same direction. It is a coupled mode involving terms decaying rapidly beneath the free surface as a surface wave and a term representing a bulk wave radiating into the solid. This mode is called "leaky" or "pseudo" surface wave. For many choices of crystal and plane of propagation, the bulk term has a small contribution. The energy of the wave is essentially concentrated within a few wavelengths of the free surface and flows parallel to the surface as with the normal elastic surface waves. Besides, in certain specific directions, the bulk term disappears completely and the pseudo-surface wave has all the properties of the normal surface wave.

2.5 Surface Acoustic Wave on (001) Plane of Cubic Crystal

Consider a surface wave of the Rayleigh type propagating on the basic plane (001) of a cubic crystal with anisotropy ratio $\eta > 1$. If the propagating direction deviates from the x axis, or [100] direction, the SAW velocity becomes more and more close to the velocity of one of the bulk shear waves which can also propagate in this direction. And the wave displacements deviate from the sagittal plane and become almost parallel to the crystal surface if the angle is close to 45^{o}. The wave penetrates deeply and degenerates into a bulk shear wave for $\theta = 45^{o}$. The phase velocity curve has a mirror symmetry about 0^{o} and 45^{o} from the [100] direction[21].

In general, there are two transverse bulk waves: One with propagation vector perpendicular to the surface does not satisfy the boundary conditions and has a nondispersive phase velocity. The other bulk wave, with the propagation vector parallel to the (001) plane in the direction as rotated, has the particle displacement not perpendicular to the sagittal plane, except at 0^{o} and 45^{o} from [100] direction. Along these directions the displacements are perpendicular to the sagittal plane and satisfy the traction-free boundary conditions. The surface wave velocity dispersion curve has lower values than those of the bulk waves, and there is a gradual degeneration of this surface wave into the bulk wave solution from 30^{o} until eventually at 45^{o} from [100], it becomes a lower transverse bulk wave.

At 0^{o} and 45^{o} from [100] direction, the solutions of the surface wave will be of pure-mode Rayleigh type. As the propagation vector is rotated from 0^{o} or [100] direction, the surface wave solution will have a term with the imaginary-axis root that becomes more and more important and this root will move closer to the origin of the complex plane, giving the solution in the forms of the bulk waves. It means that there is a deeper penetration

of the particle displacement in depth of the surface wave. It is calculated that right along the [110] direction when the wave solution has degenerated completely into the bulk wave, there is no variation in amplitude with depth. The particle displacement also evolves from the ellipse of pure-mode Rayleigh type through nonpure-mode types with particle displacement not in the sagittal plane into linear polarization at 45^{o} from [100] or [110] direction.

However, this degeneration of SAW into a bulk wave is compensated by the appearance of a special Rayleigh wave with displacements in the sagittal plane. A peculiar feature of this wave is that its velocity is greater than the velocity of one of the shear bulk waves. It is very interesting since there is no such situation in the case of isotropic media. This comes from the fact that as the angle deviates from 45^{o}, SAW is in synchronism with one of the bulk waves and radiates energy into the bulk. This coupling effect is that a SAW is accompanied by a shear bulk wave of small amplitude traveling away from the surface. And a surface wave is attenuated in the direction of propagation because of the loss of energy into the substrate.

It is interesting to note that the amplitude of this bulk wave increases with depth since the bulk waves propagate forward at an angle with the substrate surface and the amplitude of the waves radiated earlier is greater. Such a peculiar combination of surface and bulk waves is called a pseudo-surface wave or leaky wave. For small angles of deviation from [110], the attenuation of a pseudo-surface wave is very small in the direction of propagation. Such small attenuation could hardly be noticed in experiments, and pseudo-surface waves are often observed as genuine Rayleigh waves. But if the angle is exactly equal to 45^{o}, there is no longer a pseudo-surface wave since these waves cannot be coupled as one can see from the properties of symmetry. The wave at this angle is a pure-mode Rayleigh wave[21].

2.6 Surface Acoustic Wave on (111) Plane of Cubic Crystal

This (111) plane is no longer parallel to a mirror plane of crystal symmetry; therefore, the root $l_3^{(n)}$ is no longer bicubic and here we have the most general forms of normal surface wave. The phase velocity curve has a mirror symmetry about 0^o and 30^o from the [110] direction and hexagonal symmetry in general on the surface plane.

There are two transverse bulk waves propagating along this (111) plane. As the propagation directions rotate away from [110] direction to the direction of 30^o from the [110], one bulk wave with higher phase velocity has a decreasing phase velocity, while the other displays an increase in phase velocity, still with lower velocity than the former bulk wave. The calculated and measurement results give the surface wave with velocity lower than the lowest bulk wave velocity. They show that the phase velocity is a monotonically increasing function of the angle away from [110] direction, reaching the maximum at 30^o away from [110] direction.

For propagation directly along [110], the imaginary axis root of the solution is quite close to the origin resulting in the largest penetration of this solution into the bulk of the material, and the surface-wave velocity is closest to the bulk wave velocity in this direction. The particle displacement is of elliptical shape with the plane of the ellipse rotating corresponding to the roots in the solution for each propagation direction.

In contrast to the mirror plane cases where the bulk shear waves at any angle are polarized either parallel (SH) or perpendicular (SV) to the plane, in the (111) plane, the polarization relative to the plane is much more complicated except along the direction of 30^o away from [110] where the polarization of one is SH. Along the [110] direction, the

two shear modes are pure shear polarized perpendicular to the propagation direction but are not SV or SH. The bulk shear wave does not satisfy the surface boundary conditions at any angle except at 30^{o} with the SH bulk wave whose propagation vector is not parallel to the plane but tilted upward at an angle to the surface of the sample with the velocity greater that of the lowest transverse bulk-wave. In fact, this solution is an extremum of a pseudo-surface wave branch on the (111) plane.

For the surface wave, at all angles except along the 30^{o} direction where only the two sagittal plane components are present, all the three components of displacement are involved. Here, the displacement ellipse is in the sagittal plane at each depth but the two components are not in phase quadrature and thus the principal axis is not perpendicular to the free surface.

It is also expected to observe experimentally the pseudo-surface mode since the majority of the energy of this wave mode propagates within a few wavelengths of the surface but with a component propagating into the bulk material. The attenuation of this upper branch is comparatively small except near 30^{o} where the solution requires deeper penetration. At 30^{o} from [110] direction, the pseudo-surface mode degenerates into the simple bulk wave of the type with a tilted wavevector[10, 21].

2.7 Waves in Plates and Layered Structures

Now we shall move to the topic of our experimental geometry of thin film-substrate system by considering more complicated systems (plates, layers on substrate, etc.) where the characteristics of the surface wave are the result of the presence of just one sur-

face, with two parallel surfaces as in plates. This immediately increases the number of eigenmodes propagating in such systems and results in complicating their structure.

2.7.1 Love Waves

This is a shear surface acoustic wave generated by perturbations of boundaries in the layered materials. If the velocity of shear bulk waves in the layer is less than in the half-space, the shear waves can propagate in this system. Considering an isotropic system, in the case of a thin layer ($qd << 1$, where q is the wavevector and d is the film thickness), there exists only one Love mode; however, for larger values of the parameter qd, several Love modes can exist. It is the simplest type of surface waves since the calculations for the Love waves are much simpler than for the Rayleigh waves which have to be solved numerically. Weakly inhomogeneous Love waves can also exist in an elastic half-space with surface inhomogeneity. In this case, a near-surface region of the substrate acts as a layer where the velocity is less than in the remaining part of the acoustic wave propagation.

2.7.2 Waveguide Modes in Plates and Layered Structures

First consider waves propagating in a free isotropic plate. Waves of two different polarizations can propagate in a plate: pure shear waves with displacements parallel to the surfaces and perpendicular to the direction of propagation (shear horizontal or SH waves), and the pure shear waves with displacements lying in the sagittal plane. For SH-waves, they are represented as the sum of plane shear waves reflected successively from the surfaces of the plate. In the case of such polarization, the reflection will be without transfor-

mation of transverse waves into longitudinal waves. Therefore, the reflection coefficient is equal to one and the displacement can be symmetric or anti-symmetric with respect to the plane ($z=0$) which goes through the plate center.

For the displacement in symmetric mode, we have

$$u = u_0 \cos(nx) \exp[i(qx-wt)] \tag{6}$$

where $n^2 = (w^2/c_t^2)-q^2$. In particular, for $n = 0$, there exists a shear wave without dispersion propagating in the plate, and for n not equal to 0, these modes are characterized by critical frequencies and dispersion. Similarly, for anti-symmetric modes, the displacement is

$$u = u_0 \sin(nx) \exp[i(qx-wt)] \tag{7}$$

On the other hand, the modes from the bulk shear wave whose displacements lie in the xz plane or the sagittal plane are of more complicated structures. In the case of such polarizations, the bulk shear waves and the longitudinal waves transform into each other via reflecting from a free boundary. Thus, it may be considered as a set of coupled longitudinal and transverse waves and these modes are called the Lamb modes. There are also two types of Lamb modes: symmetric and anti-symmetric with respect to the plane $z = 0$ at the plate center. Lamb waves, as guided waves, will travel within flat or mildly curved plates, giving a possible path of inspection to an inaccessible area. Also because of their dispersive nature, where the propagation velocities are the function of the excitation frequency and the plate thickness, they can be devised for the measurement of the film thickness[6,13]. Lamb waves are useful in the inspection of metal and composite plates for horizontal separations, i.e. for film-substrate delamination[8].

The analysis shows that the number of modes which can propagate in a plate increases with the increase of the parameter qd where q is the wavevector and d is the plate thickness. At long wavelength or low qd, the condition is similar to that of bulk plane

waves. However, for a very short wavelength, separate waveforms are excited; in the interior, bulk waves propagate, while on the surface, Rayleigh waves are excited. For intermediate wavevectors, numerous plate modes having both symmetric and antisymmetric configuration are excited by the acoustic waves. If the value of qd is small, $qd<<1$, only two lower first modes can propagate in a plate: the symmetric mode which is a longitudinal wave and an anti-symmetric dispersion flexural wave - a combination of shear and longitudinal waves accompanied by relatively large transverse displacements. For large values of qd, the velocities of first order modes approach the Rayleigh wave velocity. The Rayleigh wave in a plate of finite thickness can be represented as the sum of symmetric and anti-symmetric first Lamb modes. However, for $d/\lambda > 5$, since the displacements in the first Lamb modes damp exponentially to the plate center, the Rayleigh waves on the other higher order Lamb modes will dominate resulting in the velocity of the transverse wave c_t as qd -> *infinity* as shown in Fig.[2].

The above theory is for the system of a free isotropic plate. Then if we consider a very thin plate as a thin film layer on a comparatively thick substrate, in other words, a thin film-substrate system, there is a much richer spectrum of eigenmodes. With the presence of a solid homogeneous film of uniform thickness d in good contact with the substrate such that the traction stress and mechanical displacement are continuous across the interface at $x_3=0$, modification in the characteristics of surface wave propagation is required. Here, the wave equation must be solved separately in each of the film layers and substrate materials as was done above, and a linear combination of the appropriate partial waves should be considered to satisfy the boundary conditions, which are the continuity of the traction stresses and the particle displacements at the interface ($x_3=0$), and the vanishing of the traction stresses at the free surface, which is now $x_3=d$.

The thin solid film layer introduces a characteristic dimension into the problem. The prominent effect of the presence of the film layer is the shift of the surface wave velocity and the dependence of this velocity on the wavevector of acoustic wave. Thus, the medium becomes dispersive, with the phase velocity depending on the ratio of the wavelength to this dimension *d*. There are three qualitatively different cases:

If a film layer is thin with respect to the wavelength ($qd << 1$), then since the distribution of particle displacements as a function of depth and the film layers elastic properties do not differ much from the substrate, there is a Rayleigh wave propagating in the system. The wave energy is mainly concentrated in the substrate since the depth penetration is greater for this relative wavelength but the wave properties are slightly modified because of the existence of the film layer. In particular, if the velocity of the shear waves in the film layer is less than in the substrate, which is called a substrate-loading case, the film layer will slow down the Rayleigh wave and it indicates SAW waveguide as of the Flat Overlay Waveguide on the infinitely wide strip[22]. If the velocity is greater, the film layer will accelerate the Rayleigh wave. It is called a film-loading case. A very rigid and heavy layer on a soft substrate can induce the wave motion typical for a flexural wave in substrates[22].

If a film layer thickness is of the same order as the wavelength ($qd = 1$) and the velocity of shear waves in this film layer is less than in the substrate, there will be several different modes with different velocities and different spatial distributions of displacements propagating in this system. Actually, they are the Lamb modes in the film layer distorted by mechanical contact with the substrate. The first of these modes related to the first anti-symmetric Lamb mode is called the *Sezawa* wave.

If a film layer is thick with respect to the wavelength ($qd >> 1$), the wave energy is mainly concentrated in the film layer since the depth penetration into the substrate is much

smaller for this relative wavelength. Two modes can be chosen from a large number of modes propagating in the system. These two modes form a Rayleigh wave running along the external boundary of the film layer, and it exists for any relations between mechanical parameters. The velocity of this wave is close to the Rayleigh wave velocity v_R in the film layer material.

Moreover, in addition to this Rayleigh wave, an interface Stoneley wave can also propagate along the interface of the layer and the substrate for certain relations between the film layer and substrate parameters. In some anisotropic crystals a Stoneley wave can also be a pure shear wave[19].

From a typical dispersion curve for the surface wave propagating in a film layer of fixed thickness which displays a substrate-loading case, it is seen that with increasing frequency the phase velocity ω/q changes gradually from that of the Rayleigh wave on a free surface of the substrate to the value of the Rayleigh wave velocity on a free surface of the film layer material. The group velocity of this wave is equal to the phase velocity for zero thickness ($qd=0$) and for large values of qd, but for intermediate values of qd, the group velocity will differ from the phase velocity due to the dispersive behavior.

Higher order modes of propagation in a layered medium always exist for sufficiently large values of qd. The dispersion curve will display cut-off values which are the frequencies observed where some of the phase velocities of the higher order modes approach infinity. Each higher order mode has a cut-off value of qd at which its phase velocity matches that of a bulk shear wave propagating parallel to the surface. The penetration into the substrate of the coupled wave becomes very deep and the group velocity equals the phase velocity. For values of qd larger than the corresponding cut-off qd value, the phase velocity of these higher modes decreases dispersively until at very large qd, it becomes asymptotic to the velocity of a bulk shear wave in the film layer material.

For a value of qd very close to the cut-off value, the vertical displacement component has a constant amplitude at large depths so that this wave of higher order modes close to the cut-off might be described in terms of a SV bulk wave perturbed by the surface boundary conditions. As the value of qd becomes much greater than the corresponding cut-off value, these higher Rayleigh modes have a character close to that of a plate mode of thickness d of the film layer material, but with the small perturbations by the existence of the substrate below $x_3=0$, and there will be a small fraction of energy carried into the substrate.

In addition to Rayleigh modes, there are also Love modes. For values of qd near cut-off, the penetration of Love waves is very deep into the substrate and a large fraction of the energy of the wave is carried in this substrate. As qd increases so that the wavelength becomes less than the layer thickness, the displacement profiles approach those of a plate free on one surface and clamped on the other, but with a small perturbation in the interface region.

If the film layer or the substrate is anisotropic or piezoelectric; the solutions are much more complex in that they do not just separate into pure-mode Rayleigh and Love waves. The general solutions including the potential and all three components of displacement in both the film layer and the substrate need to be solved for complete particle displacement and dispersive behavior. Still, we tend to categorize the solutions in terms of Rayleigh-type and Love-type waves considering the components of polarization patterns.

Chapter 3: Impulsive Stimulated Thermal Scattering

Fig.[3] shows the schematic of the experimental setup called Impulsive Stimulated Thermal Scattering (ISTS). ISTS experiment is comprised of two parts: The excitation laser pulse and the probe laser pulse. The excitation component started from the output of a Q-switched, modelocked, and cavity-dumped Nd-YAG laser. It is a 1064 nm wavelength pulse of 100 picosecond duration at a repetition rate of 100 Hz. Note that the repetition rate is adjusted so that it is high enough to minimize the noise compared to the signal level and low enough to allow the surface thermal relaxation to completely finish between each laser shot. Then the light is attenuated and passed through Lithium Triborate (LBO) crystal which gives the outgoing wave of 532 nm for the excitation beam. This second harmonic light is then attenuated to 10 μJ pulses before passing through a cylindrical lens and changed to an elliptical spot size to be 1.5 mm horizontally and 400 μm vertically on the phase mask pattern which consists of evenly spaced grooves etched onto a glass substrate. The phase mask splits the beam into many diffraction orders with the energy mainly confined in the first diffraction orders. Both of the first diffraction order beams travel through a set of two plano-convex spherical lenses with focal distances $f_1=25\ cm$ and $f_2=15\ cm$ which gives a 5:3 imaging system of the phase mask onto the sample.

The phase mask application has been introduced and developed by *Rogers et al*[26] to provide a compact and simple optical setup for the spatial and temporal crossing of the excitation laser pulses at the sample surface compared to a conventional beam-splitting method. It creates a sinusoidally varying interference pattern on the sample with a wavevector $q=2\pi/\Lambda$ where Λ is a grating fringe spacing which could be deduced by the imaging ratio to the phase mask fringe spacing. The absorption of the light at the bright area of the interference pattern results in an immediate spatially periodic heating on the

sample surface. Then, thermal expansion gives rise to variation in density of the sample, and thus the acoustic wave is launched. For this particular ISTS experiment, we would observe acoustic wave penetration which is approximately one acoustic wavelength deep below the surface. Simply changing the mask patterns allows us to vary the excitation wavelength, and thus the depth-dependence of the excitation can be arranged. Since we set up the experimental geometry so that the sample has two acoustic waves propagating in the opposite direction to each other, the acoustic waves undergo standing-wave oscillations with damping in amplitudes followed by thermal decay on a longer time scale.

The excited material motions are monitored in real time by a probe laser pulse. The probe laser is a cw, single-mode Argon ion laser. It generates a 514 nm wavelength output of 0.5 Watt with a flat intensity profile. It is then electro-optically gated to a square pulse with an adjustable temporal width from 50 ns to many seconds. The probe laser pulse is diffracted by the material motions, and reflects from the sample. Here, the reflective mode of diffraction is monitored and the first order diffracted response is collected through the fast, amplified photodiode (*Hamamatsu C5658*, 1GHz bandwidth) and displayed on a transient digitizer (*Tektronix DSA 602A*, 1 GHz bandwidth).

In this experiment, we arranged a heterodyne setup by passing the probe through the same phase mask at the same spot as the excitation. At the mask we measured the spot size of the probe Ar laser beam to be a round spot of 140 μm in diameter. Hence, the probe beam is also diffracted into two orders, the "probe" and "reference" beams, which are recombined at the sample with the same imaging system as the excitation beam.

With this setup, the sample is always probed at Bragg angle and the diffracted signal from the probe beam is reflected off the sample coincident with the reflection of the reference beam[24]. One great advantage for this heterodyne setup is that for a particular sample which typically yielded very weak signal, such as for a Ti film, the signal is easily

seen and aligned for optimization. Furthermore, the intensity of signal response from the photodiode is not the square of the acoustic response amplitude anymore, rather the square of the sum of the amplitude of the diffracted signal and the reflected probe reference amplitude. Generally, the amplitude of the reflected probe is much greater than the amplitude of the diffracted signal so that the crossing product plus the reflected intensity is the dominant term for the signal response intensity, resulting in a much higher signal response from the photodiode.

Here the importance of the accuracy in the wavevector measurement should be noted since the wavevector q value is required to calculate each acoustic velocity. We determined the grating wavevector by calculating the acoustic wavelength from the known acoustic velocity of pure water and the measured acoustic frequency of very diluted $KMnO_4$ solution which strongly absorbs the excitation pulses and yields good signals.

The absolute displacements and the diffracted signal will decrease with increasing wavevector q; therefore, the signal intensity decreases as the excitation angle (or wavevector) increases. Waveguide modes are excited and monitored in ISTS providing us a dispersion curve. For a given qd value, there will be many waveguide modes and each mode associates with different propagation velocities and spatial characteristics[14].

The phase velocity of a given mode at different wavevectors q can be considered as a depth dependent probe of material properties. At large $qd >> 1$, the wavelength is small and the waveguide modes resemble Rayleigh waves which travel on the surfaces of film materials. As the wavevector q increases, the mode displacements become less and less affected by properties of the film near the substrate as they become localized to the surface of the film. On the other hand, as the wavevector q decreases, or the acoustic wavelength is bigger, the surface wave can penetrate to a deeper level into the substrate. At the very low

wavevector q, as the limit, the waveguide mode will resemble Rayleigh waves which travel on the surfaces of substrate materials.

Chapter 4: Results and Discussions

4.1 Surface Acoustic Wave on Ti Film Coated on Si Wafer

First of all, the samples we used for the study of waveguide effects on the anisotropic substrate are Ti thin films on Si wafers. The integrated circuit fabrication industry currently uses a single crystal Si wafer which displays high anisotropy and stiffness as a major substrate, and Ti film plays an important role as a contact layer for interconnect.

Two types of wafers have been used to observe the propagation of SAW on different planes of Si single crystal. Here, Si(001) and Si(111) *n*-type wafers have been laminated with Ti thin film by the e-beam evaporation method. Acoustic waves are launched in various directions along each plane and the waves propagate deep into the sample about one acoustic wavelength. Material motions excited by the acoustic waves resulting in the ripples on the surface will diffract the probe Ar laser beam.

We detected the probe signal from the first diffraction order of reflection mode and only the SAWs of Rayleigh type and the Leaky-type were observed. Fast Fourier Transformation was then performed on the signal responses to obtain the acoustic frequency. Fig.[4] illustrates an example of signal responses and the resulting acoustic frequency from the FFT peak from Ti film on Si(001) at [100] direction for $qd=0.45$. The form of the signal indicates the photothermal and photoacoustic responses not only from the metal film material but also from the air since the immediate heating also occurs in the air and acts as a diffraction grating from the air. There is a damping in acoustic frequency from the film material first on the fast time-scale, followed by the acoustic damping in the air. Then the thermal relaxation takes place in a longer time scale.

Longitudinal waves, quasi-transverse waves and surface waves are excited in the sample materials. It has been established by the polarization pattern that a pure-mode Rayleigh wave induces the particle displacements along the sagittal plane which is the plane along the propagating direction and perpendicular to the surface, while a pure-mode Love wave induces the particle displacements perpendicular to the propagating direction and parallel to the surface as in isotropic substrate. However, in an anisotropic substrate, when the acoustic wave propagation direction is rotated, the particle displacements are of elliptical shapes whose principal axes do not lie either strictly perpendicular to the propagating direction and parallel to the surface as in a pure-mode Love wave, or on the sagittal plane as in a pure-mode Rayleigh wave. Rather the principal axes lie in a direction that tilts away from the surface. At any angle, the observed acoustic waves are mixed modes in between the pure-mode Rayleigh wave and pure-mode Love wave. Hence, we categorized a particular propagating acoustic wave depending on the degree of tilting of displacements or the polarization pattern into two families. If there is a greater component of the Love wave character, it is called Love-type and if there is a greater component of the Rayleigh wave character, it is called Rayleigh-type.

The ISTS technique provides a symmetric acoustic wave excitation that cannot generate a pure shear wave. The contribution on the diffraction to the probe signal response comes from the pure-mode Rayleigh component. Therefore, provided that a particular surface acoustic wave has a pure-mode Rayleigh component, its acoustic response still can be detected as long as the displacement amplitudes cause surface ripples along the sagittal plane for probe diffraction to generate a signal.

Here we assumed Ti film as a homogeneous isotropic layer and Si as a single crystal with anisotropy ratio (η) = *1.57*. Angular dependence of the acoustic phase velocities

shall be expected along with the dispersive behavior from the waveguide effect since it is a typical substrate-loading case with the presence of the film layer.

As a result, the waveguide and anisotropic effects on acoustic velocities in Ti film on both Si(001) and Si(111) at different values of *qd* have been observed and compared to the calculated values. First, the difference of the velocities between the coated and uncoated Si substrates will be considered. The dispersive behavior is expected from the presence of the film. As the *qd* value is increased, the system should display less variation in the acoustic velocities, i.e. smaller anisotropic effect. Moreover, in the angular dependence curve, the characteristics and evolution of pseudo-surface waves in connection to the first and second waveguide modes will be discussed. In the dispersion curve scaled with *qd,* the so-called cut-off value as well as the coupling between the higher order waveguide modes will be considered. Finally, the accuracy of the ISTS technique over the measurement for mechanical properties of thin film materials will be taken into account.

4.2 Surface Acoustic Wave along (001) Plane of Ti/Si System

4.2.1 Angular Dependence of Surface Acoustic Velocity on Si(001) Plane.

Fig.[5] illustrates the calculation results for the angular dependence of surface acoustic waves on a pure anisotropic Si crystal in addition to Figs.[6-9] which show the measurement results along with the calculated phase velocities of SAWs along (001) plane. Similar trends for angular dependence of phase velocities are observed on each acoustic wavelength launching on the surface (or *qd*). In general, the velocity curve has a mirror symmetry at 0^{o} and 45^{o} from [100] direction.

For *qd=0.23* in Fig.[6], let us consider the wave propagating along [100] direction. The observed surface acoustic velocity at this angle on (001) plane is the lowest. As the propagation direction rotates away from [100] direction, the observed surface acoustic velocity increases monotonically until the propagation direction reaches 30^{o} from [100] direction. At this direction and a couple of degrees away, two values of surface acoustic wave velocities were observed before the observed surface acoustic wave shifted to the higher value and seems to remain constant until it reaches [110] direction or 45^{o} away from [100] direction. This is also confirmed by Fourier Transformation which yields two distinctive peaks close to each other as in Fig.[10].

We may explain this anisotropic behavior of surface acoustic waves from the calculations we have displayed also in Figs. [6-9] as a possible solution of the surface acoustic wave. Two angular dependence curves have been calculated. The one with the lower value is of the first waveguide mode while the other with the higher value is of the second waveguide mode.

Note from the previous section that the lower transverse bulk wave values at [100] and [110] directions are the bulk waves that actually satisfy the surface boundary condition and are of the pure-mode Love wave. The jump in the surface acoustic velocities at the angle around 30^{o} from [100] direction that we observed is due to the degeneration of the polarization patterns of surface waves from Rayleigh-type waves into the lower bulk shear waves of pure-mode Love-type in the lower curve of the first waveguide mode. It is noticeable especially in conjunction with the degeneration of the polarization patterns of the upper curve of the second waveguide mode from Love-type waves into the waves of Rayleigh-type that leads to the observable data from ISTS measurements since the horizontally polarized component of pure-mode Love wave may not be probed.

In fact from the fundamentals of wave propagation, when two waves of the same phase velocity meet, the coupling effect would take place which results in two different waves with higher and lower phase velocities in the upper and lower modes. One interesting point is that from these continuous plots of angular dependence of the observed acoustic velocities of these Rayleigh and Love-type curves in Fig.[6-9], instead, it yields two different curves which appear not to intersect with each other despite the fact that from the analysis of each wave type, there is an interchange in the wave characteristics between 30^{o}-35^{o} from the [100] direction at which the crossing point is expected and the walk-over of the experimental data is observed as we continued measuring the acoustic velocity for bigger angles away from [100] direction.

However, the observed values of acoustic velocity in the upper branch are not considered to be genuine surface waves, rather pseudo-surface waves since the waves are actually attenuated along the surface. As we have discussed earlier, that we observe the pseudo-surface waves although they are not real surface wave solutions is due to the fact that the energy-radiating terms in the pseudo-surface waves are relatively small so they can propagate along the surface for a long range and be detected as if they are real surface waves. Indeed, right at [110] direction, the observed surface wave becomes a pure-mode Rayleigh wave again.

The same anisotropic behavior is expected for higher *qd*. We may compare the experimental results in Figs.[6-9] to the calculated values when $qd=0$ or pure Si substrate, Fig.[5], which displays pure anisotropy. Since we assume that the film is isotropic and the material excitation regime is about one excitation wavelength below the surface, higher *qd* means greater film thickness compared to the excitation wavelength, and more contributions to the acoustic responses are from the film layer. With higher *qd*, the anisotropy effect should be lower, in other words, the variation in the observed acoustic velocity

should be smaller. The observed values are indeed as expected, when compared to the anisotropy plots on different *qd* (*qd=0.31, 0.55, and 0.86)* in Fig.[7-9] to the values from an uncoated Si substrate in Fig.[5]. As *qd* is higher, the variation between the highest velocity of the surface wave and the lowest at [100] direction is monotonically decreased.

4.2.2 Dispersive Behavior of Surface Acoustic Wave on Ti/Si(001) System

Another remark from Fig.[5-9] is that the relative values of surface acoustic velocities are apparently slower for higher *qd.* It is from the waveguide effect resulting in the dispersive behavior due to the presence of the film as extensively illustrated in Fig.[11-16]. Here, the dispersion curve relates the acoustic velocity to the scaling product of the wavevector q and the film thickness d. The film-substrate materials may contain acoustic waves of more than one waveguide mode with the number of modes allowed to propagate depending on the *qd* value. At higher *qd* or relatively higher film thickness to the acoustic wavelength, more modes can propagate and each mode associates with a different phase velocity and spatial character.

When the acoustic wavelength is much bigger than the film thickness, i.e. small value of *qd*, material motions will be mainly confined in the substrate giving the signal responses similar to those from the bulk material limit of the substrate material which show the Si substrate surface and transverse velocities. With the decrease in acoustic wavelength, until the wavelength is comparable to or less than the film thickness, the film layer will act as an acoustic waveguide which can support many acoustic modes. The dispersion curves contain several waveguide modes from *qd=0* to *qd=10* are illustrated in Figs.[11-14]. Actually, in our experiment focusing on typical thin-film applications for

microelectronics where the thickness of the film is up to 0.5 μm, we may sufficiently limit our study of the dispersive behavior of such a system to a regime up to $qd=1$ where only the first two modes may propagate since the values of q or wavevector are limited by the phase mask spacings which are required to be on the order of the excitation laser wavelength.

Recall from the isotropic model that the surface acoustic waves are pure-mode Rayleigh-type in the first waveguide mode and pure-mode Love-type in the second mode; therefore, the calculation of dispersion curves only on the first waveguide mode will be sufficient for ISTS measurement. However, from the study of anisotropy there is a regime of the propagating orientations where the observed surface waves are pseudo-surface waves lying on the second waveguide mode. Therefore, it is obviously important that the first two surface acoustic waveguide modes are presented in the dispersion curves for the fitting process, rather than only one mode as in the isotropic case.

Regarding the dispersion curves in Figs.[11-14], when $qd->0$, only the first two modes of Rayleigh-type wave and Love-type wave can propagate in the film system. With higher qd, several higher order modes may occur. First, in an isotropic system, when no film is coated on the surface or $qd=0$, it is expected to find the phase velocity of the Rayleigh-type wave in the first mode to be that of the substrate Si surface velocity and the phase velocity of the Love-type wave in the second mode to be that of the substrate Si transverse velocity. Both values are the same for any orientation. However, in an anisotropic system, the surface wave for $qd=0$ limit of the uncoated substrate which is the surface wave of Si in the first waveguide mode would be different for different propagation directions due to the anisotropy effects as mentioned above. Besides, at particular orientations where pseudo-surface waves are observed, the $qd->0$ velocity limit for the second waveguide mode is observed to be the pseudo-surface velocity in the substrate Si, rather

than the lower transverse velocity. Indeed, the difference in the *qd->0* velocity limit for the second waveguide mode as expected in isotropic compared to anisotropic model is explicitly seen here.

Starting from *qd=0* where all the acoustic responses are from the substrate, the bigger the *qd* value the more the acoustic responses are from the film, until *qd* approaches infinity which poses the limit of the dispersion curve that acoustic responses will be entirely from the film. When the film is so thick on the substrate, the velocities of the first and second waveguide modes should approach those of the Ti film surface wave and transverse bulk wave respectively. For the *qd* value in between these extreme cases, there will be a gradual change in phase velocity due to the waveguide effect.

First let us consider the acoustic responses along the [100] direction in Figs.[11-12]. The shear acoustic velocity and the surface wave velocity along the Si(001) on the [100] direction are 5,844 m/sec and 4,917 m/sec respectively and they will be the first values of the dispersion curve calculation when *qd=0*. For *qd<1*, only the first two modes can propagate. As *qd* increases, the number of the waveguide modes will increase. The sixth mode may propagate at *qd=10*.

It has been interpreted that the so-called cut-off value in the dispersion curve for higher order waveguide modes at higher *qd* values represents the value of the wave propagating along the surface when its phase velocity is equal to that of the lower transverse bulk wave propagating along the surface, and satisfies the surface boundary condition at a particular direction. Here, we note that the velocities at these cut-off values for higher order modes in Fig.[11] are equal to the velocity of the substrate Si transverse velocity of 5,844 m/sec since at this angle, each higher order mode would have its phase velocity match to that of a pure-mode Love wave. Particularly at this [100] direction, the particle motion for Love-type wave is perpendicular to the propagation direction and parallel to

the surface. However, the ISTS technique provides no excitation or detection of this pure-mode Love-type wave in the second waveguide mode; therefore, only the Rayleigh-type acoustic wave is observed in the first waveguide mode which is also a pure-mode at this [100] direction. As in Fig.[11], we shall see that the observed velocities of this surface Rayleigh wave correspond very well to the calculated values. The velocities of both waveguide modes drop for higher values of qd, i.e. as the film becomes thicker. At very large qd, the acoustic velocity of the first waveguide mode becomes asymptotic to the velocity of the surface Rayleigh wave of the Ti film ($v_{Rf} = 3{,}014\ m/sec$) and the acoustic velocities of all other higher waveguide modes approach the lower transverse bulk velocity of the Ti film ($v_{Tf} = 3{,}125\ m/sec$).

Similar trends of the calculated dispersion curves of several waveguide modes are obtained for other directions of acoustic wave propagation as seen in Figs.[13-14]. Notice that the values of the calculated velocities are modified by the anisotropy effect as discussed above. Although the observed values from the ISTS experiment are consistently matched with the calculated values, the observed acoustic waves correspond to different waveguide modes. In the [110] direction in Fig.[13], the surface wave of the first waveguide mode degenerates into the lower transverse bulk wave of Love-type and the pseudo-surface wave or Leaky wave is detected. Therefore, the experimental plots lie on the upper velocity values of the second waveguide mode curve in Figs.[13-14]. It is necessary to clarify that this pseudo-surface wave or Leaky wave is observed from the ISTS experiment because it has a significant component of the pure-mode Rayleigh wave.

One good analogy is to consider these first two waveguide modes in anisotropic materials as evolved from the Rayleigh and Love branches of the first Lamb mode in isotropic materials. By the nature of anisotropic behavior, at a particular angle when the wave supposedly in the Rayleigh-wave curve develops its particle displacements into a non-pure

Rayleigh-type mode and the wave supposedly in the Love-wave curve develops its particle displacements into a similar manner of the same phase velocity, the coupling effect may result in the splitting of these first Lamb modes of Rayleigh and Love waves into the first and second anisotropic waveguide modes. Thus, from the result of the coupling effect, the pseudo-surface wave which possesses a larger component of the pure-mode Rayleigh character appears in the second waveguide mode branch with the velocity above the so-called cut-off value.

Here we should stipulate the relationship between pseudo-surface waves or Leaky waves and the so-called cut-off value of several acoustic modes, which has not been noted by *Farnell and Adler*[15]. The pseudo-surface wave or Leaky wave is the wave of Rayleigh-type character which can propagate with velocity higher than the lower transverse velocity or the so-called cut-off velocity defined at a particular angle. It is true that no real surface acoustic wave is expected with velocity higher than the so-called cut-off velocity. But that does not mean that no wave can be observed above that value, and in fact from the calculation as well as from the experiment, we observed the pseudo-surface wave of higher order acoustic waveguide modes at velocities higher than the so-called cut-off velocity. It appears continuously and extensively from the cut-off qd value until it reaches another velocity limit at $qd=0$ which is the pseudo-surface velocity of the Si substrate material. The reason it is called the Leaky mode is because the energy of the wave is attenuating along the surface unlike those true modes for which no energy is attenuated along the surface. Thus, the starting point of the true-surface wave mode is below the cut-off value. The observation of the Leaky type wave as a surface wave is due to the small attenuation rate of energy. We shall again address what we found here that the $qd->0$ velocity limit is the pseudo-surface velocity on the substrate, not the substrate transverse velocity as in the isotropic case.

As pointed out earlier in the anisotropy section concerning the coupling effect, it is believed that there is a particular value of *qd* in the dispersion curve at which two surface acoustic waves propagating along the surface should have the same velocity. Two curves of higher and lower waveguide modes appear not to intersect with each other despite the interchange in the wave characteristics of each mode at the *qd* values higher than the *qd* value at which the crossing point is expected. As in Figs.[13-14], the coupling behavior may be observed from the calculation in the vicinity of *qd=1* for the first and second waveguide modes and at higher *qd* for other higher-order pairs of acoustic waveguide modes. It is shown that for orientations in which the acoustic waves from the first two modes may simultaneously be observed, the dispersion curve of the first mode does not actually split into two branches at a certain *qd* close to 0 as suggested by *Mourad et al.*[25]. Rather, there are initially two branches of the first and second waveguide mode for each value of *qd*.

As *qd* is higher, the acoustic waves are localized nearer to the surface of the film. They are like the surface waves in isotropic materials as the degree of isotropy increases where only pure-mode Rayleigh waves and pure-mode Love waves can propagate, not pseudo-surface waves. Consequently, this interpretation might further explain the reasons for the disappearance of pseudo-surface waves in the report of *Aono et al.*[26]. Besides, from the coupling effect, we may understand why the velocities of the pseudo-surface waves are always greater than that of the lower transverse bulk wave in the same orientation.

4.3 Surface Acoustic Wave along (111) Plane of Ti/Si System

4.3.1 Angular Dependence of Surface Acoustic Velocity on Si(111) Plane

As mentioned earlier, the most general forms of normal surface wave are expected for propagation of surface acoustic waves along this plane. The shear and surface wave velocities for propagation on the (111) plane have approximately mirror symmetry at the angles 0^o and 30^o from [110] direction, or hexagonal symmetry on the surface plane. Figs.[16-17] illustrate the observed and calculated phase velocities of waves with propagation vector parallel to the free surface along the (111) plane as a function of angle from the [110] direction for two different *qd* values (0.26 and 0.55), compared to the uncoated substrate of pure anisotropic Si in Fig.[15].

It is seen from the calculation that there are always two modes of waves propagating along the surface. The first waveguide mode is the surface acoustic wave and the second waveguide mode is the pseudo-surface or Leaky wave. These two modes are observable except for the Leaky wave at the angle close to the [112] direction or 30^o from the [110] direction where the energy-radiating terms become so large that they cannot be detected as surface waves. A monotonic increase in surface acoustic wave velocity from [110] direction to [112] direction is observed which fits very well with the calculation values.

A similar trend of angular dependence of the phase velocity is observed at different *qd* in Fig.[16] compared to Fig.[17]. For higher *qd*, the variation between the highest velocity of the surface wave and the lowest at the [100] direction is smaller, due to the smaller depth penetration of the acoustic waves into the anisotropic substate. The relative value of surface acoustic velocity will be slower because of the dispersive behavior due to the presence of the film.

4.3.2 Dispersive Behavior of Surface Acoustic Wave on Ti/Si(111) System

First let us consider the acoustic response along the [110] direction in Figs.[18-19]. The pseudo-surface acoustic velocity and the surface wave along the Si(111) on the [110] direction are 5,581 m/sec and 4,539 m/sec respectively. The trends of the dispersion curves are quite similar to what was previously discussed in that only the acoustic waves from first two waveguide modes can propagate at low *qd* while higher order modes may coexist at higher *qd*. The behavior of the so-called cut-off values is also similar to the previous case in that for the higher order waveguide modes, the cut-off velocity is the lower transverse bulk wave velocity of the Si substrate along the (111) plane on [110] direction which is v_{Ts}= *4,670 m/sec*. Here also is confirmed the fact that the pseudo-surface wave branch is a *qd->0* limit for the second-order acoustic waveguide mode.

From Figs.[18-19], both the surface Rayleigh waves and pseudo-surface waves are detected and the variation in the velocity of the dispersion curve due to the waveguide effect on the acoustic wave is illustrated. The observed data recorded from two films of different thicknesses and several wavevectors, and the calculated velocities correspond very well with each other. We adjusted for an uncertainty factor of 1.35 in the value of thickness of one film sample based on uncertainties in thicknesses observed in the SEM results, so that the results from the two samples agreed in overlapping *qd* ranges. As we rotate the propagation direction to the [112] direction as for Figs.[20-21], the relative velocity of the acoustic wave for the Rayleigh-type wave will be higher while no more pseudo-surface wave is detected since it degenerates into a pure-mode Love wave at this angle as discussed in the previous section on anisotropy effects.

4.4 ISTS Measurement for Higher Accuracy

In ISTS, measurement of the acoustic frequency on a sample surface with known acoustic wavelength from the experimental geometry leads to the determination of the acoustic velocity. In general, the acoustic velocity depends on material elastic moduli and density. The anisotropy plays an important role in the values of the elastic moduli which results in the variations of the expected acoustic velocities along a particular plane at different orientations. The dispersion curves act as a standard for a curve-fitting process that relates the acoustic velocities with scaling parameters qd, since the value of wavevector q is already known by the experimental geometry. We may exploit the ISTS technique in many different ways to determine the physical or mechanical properties of the film material[8, 13, 14].

In many cases, either we know the film thickness and measure the acoustic velocities to calculate the elastic moduli, or we know the elastic moduli and measure the acoustic velocities to calculate the film thickness. The propagation direction of the excited acoustic wave should become a noticeable factor if higher accuracy is required, especially in the nanotechnology industry. This might not be the case for isotropic materials. Yet, most of the materials in microelectronic applications display anisotropic properties. The isotropic model may prove to be insufficient, as is shown in Fig.[22]. The calculated velocities from the isotropic model are substantially different from those from the anisotropic model. In this study of anisotropic effects, theoretical analysis for calculating acoustic modes of a supported film for an arbitrary orientation, along with the experimental technique featuring optically heterodyned signal detection may provide an adequate basis for accurate characterization of thickness and elastic properties of thin films on anisotropic substrates.

Chapter 5: Preliminary Study on Damascene Structure

The main content in this thesis has focused on the study of the waveguide effect in anisotropic substrate materials. The results display a good agreement between theory and experiment which indicates that we may have an adequate basis for thin film characterization on such an anisotropic substrate. This leads to the motivation for further analysis of the physical and mechanical properties of other complicated structures such as Damascene which is currently of great attention. It might be one of the breakthroughs for miniaturization in integrated circuit fabrication using copper as a prominent conducting material.

Damascene Structure for this experiment consists of a series of vertical bars of Cu parallel to each other with different bar widths and spacings between bars. Generally, the bar width is about 1 μm and the bar length is about 3 mm. Between each bar is a layer of silicon dioxide with a thickness of 0.1-0.4 μm. The serpentine and comb structure of copper is subjected to a chemical mechanical polishing process. This unique geometry adds an interesting element to the ISTS technique since it also provides a permanent physical grating in the sample which may introduce further interactions or peculiar phenomena in the experiment.

The difference in the geometry of Damascene obviously emphasizes the increasing influence of the waveguide effect on the observed acoustic velocity since now the scaling parameter should not be only the value of the film thickness compared to the excitation acoustic wavelength but also the value of bar width since its dimension approaches that of the acoustic wavelength. The propagation direction of the acoustic wave, whether it is along the trench or across the trench, is also an interesting issue.

As a preliminary study, we simplify the experiment by exciting the acoustic wave only along the trench direction and see the variation of the acoustic velocity upon chang-

ing the structure geometry. The parameters of the geometry provided for the sample we acquired are the specific density, which is the ratio of the area of Cu material to oxide material on each pattern, and the widths of the bars.

In Figs.[23-24], we compare the acoustic responses from patterns with the same specific density but different bar widths and notice that the acoustic velocity is lower for a bigger bar width. Next, we compare the patterns of the same bar width but different bar spacings or different specific densities and the acoustic responses are observed in Figs.[25-26]. It is shown that the acoustic velocity is also lower for higher specific density.

The oxide layer is transparent to the excitation light. Our excitation model for Damascene is as if several parallel strips of Cu lie on the substrate Si and the waveguide effect should be similar to the Strip Waveguide model in which this Damascene mass-loads the Si substrate[22]. Yet, it will be more complicated if the acoustic waves along the bars would feel or interact with each other. Also, the anisotropy effect from the Si substrate and the permanent grating geometry of Damascene itself should not be neglected; thus, the acoustic responses from the excitation along the trench and across the trench are expected to be different.

From this preliminary experiment, dispersion curves that can be used as standard curve-fitting for the physical and mechanical properties of Damascene are ultimately expected. However, we need several different types of Damascene in order to understand the dispersive behavior and construct dispersion curves with all the scaling parameters.

Chapter 6: Conclusions

The ISTS technique provides thermal excitation on sample materials which launches counterpropagating surface acoustic waves. With knowledge of the experimental geometry and measurement of acoustic frequency, the acoustic velocity is determined. Further information on either the elastic moduli, the film thicknesses, or the adhesive degree of the sample materials may be calculated by fitting all the relevant parameters to the dispersion curves set as standard. Here, the anisotropy effects in thin metal films have been studied. The variations of the acoustic velocities along each particular plane of propagation are modified into standard dispersion curves for the fitting process.

As the scaling parameter qd is higher, the material motions tend to be localized more in the thin film materials, and the variations of the acoustic velocity in the first and second waveguide modes due to the anisotropy effect are smaller. The modified dispersion curves of the film system along the Si(001) plane and the Si(111) plane with the anisotropy effect are presented. We measured the acoustic responses and they correspond very well to the modified dispersion curves. These modified dispersion curves are compared to the dispersion curves previously calculated by using the isotropic model and it has been shown that for films of submicron thickness or $qd<1$, the anisotropy effects on acoustic velocities are substantial.

Moreover, by observing different acoustic waveguide modes in the dispersion curves and angular dependence curves, particularly in the Si(001) plane, there is a range of angles where surface acoustic waves from the first and the second modes are simultaneously detected. The interchange of the surface wave characters between Rayleigh-type wave and Love-type wave in the first and second modes indicates the coupling effect.

In addition, the relationship between the cut-off value of higher order waveguide modes and pseudo-surface waves has been shown. Although it has been conventionally assumed that the surface acoustic waves with velocities higher than the cut-off velocity of each waveguide mode should not propagate considering the boundary condition, in fact, the waves with such higher velocity may actually propagate despite the fact that they might not be called real surface waves, but pseudo-surface waves. The appearance of the pseudo-surface waves is always observed in the second waveguide mode branch above the so-called cut-off velocity of each mode while displaying the wave character of Rayleigh-type due to the coupling effect.

In the isotropic case, it is sufficient for ISTS technique to consider only the first waveguide mode which is of pure-mode surface Rayleigh wave. However, in the anisotropic case, for surface acoustic waves propagating along a particular orientation, the measurement observed pseudo-surface waves in the second acoustic waveguide mode. Therefore, it is important that the modified dispersion curve include the second acoustic mode. It is also established that the $qd->0$ limit for the acoustic velocity of this second waveguide mode is in fact the pseudo-surface velocity of the uncoated substrate, rather than the lower transverse velocity as in the isotropic case. In this study, we provided an adequate basis for accurate characterization of thickness and elastic properties of thin films on anisotropic substrates by considering acoustic modes of supported films for arbitrary orientation.

In the preliminary study on Damascene Structure, it is observed that waveguide effects from the geometry of Damascene patterns play an important role in the acoustic velocities observed. It is shown that the widths of the bar structures and the spaces between the bar structures have to be included in the scaling parameters for dispersion curves.

References

1. D. E. Bray and R. K. Stanley, *Non-destructive Evaluation: A Tool for Design, Manufacturing, and Service*, (McGraw-Hill, 1989).
2. J. B. Hull and V. B. John, *Non-destructive Testing*, (MacMillan Education, London, 1988).
3. R. Truell, C. Elbaum, and B. B. Chick, *Ultrasonic Methods in Solid State Physics*, (Academic Press, New York, 1969).
4. J. de Klerk, in *New Directions in Physical Acoustics*, (Societa Italiana di Fisica, Italy,1976).
5. S. I. Rokhlin and T. E. Matikas, MRS Bulletin, **21** (10), 22 (1996).
6. Lord Rayleigh, Proc. London Math. Soc. **17**, 4 (1885).
7. J.V. Biryukov, Yu V. Bulyaev, V. V. Krylov, and V. P. Plesky, *Surface Acoustic Waves in Inhomogeneous Media*, (Springer-Verlag, Berlin, Heidelberg, New York, 1995).
8. J. A. Rogers and K. A. Nelson, J. Adhesion **50**, 1 (1995).
9. I. Viktorov, *Rayleigh and Lamb waves*, (Plenum, New York, 1967).
10. G. W. Farnell, in *Physical Acoustics*, edited by W. P Mason and R. N. Thurston (Academic, New York, 1970), Vol. 6, p. 109.
11. F. R. Rollins, T. C. Lim, and G. W. Farnell, Appl. Phys. Letters **15** (12), 236 (1968).
12. R. G. Pratt and T. C. Lim, Appl. Phys. Lett. **15** (12), 403 (1969).
13. J. A. Rogers, L. Dhar, and K. A. Nelson, Appl. Phys. Lett. **65** (3), 312 (1994).
14. J. A. Rogers and K. A. Nelson, J. Appl. Phys. **75** (3), 1534 (1994).
15. G. W. Farnell and E. Adler, in *Physical Acoustics*, edited by W. P Mason and R. N. Thurston (Academic, New York, 1972), Vol. 9, p. 35.
16. K. Sezawa, "Dispersion of Elastic Waves Propagating on the Surface of Stratified Bodies and on Curved Surfaces," *Bulletin of the Earthquake Research Institute*, **3**,1 (1927).
17. T. C. Lim and G. W. Farnell, J. Appl. Phys. **39** (9), 4319 (1968).
18. V. R. Velasco and F. Garcia-Moliner, J. Phys. C: Solid St. Phys., **13**, 2237 (1980).
19. R. Burridge, Quart. Journ. Mech. and Appl. Math., **13** (2), 218 (1970).
20. J. L. Synge, J. Math. Phys. **35**, 323 (1957).
21. T. C. Lim and G. W. Farnell, J. Acous. Soc. Amer. 45 (4), 845 (1969).
22. A.A. Oliner, *Acoustic Surface Waves*, (Springer-Verlag, Berlin, 1978).
23. J. A. Rogers, M. Fuchs, M. J. Banet, J. B. Hanselman, R. Logan, and K. A. Nelson, Appl. Phys. Lett., **71**, 225 (1997).
24. A. A. Maznev, K. A. Nelson, and J. A. Rogers, to be published.
25. A. Mourad, C. Desmet, and J. Thoen, Appl. Phys. Lett., **69** (15), 2169 (1996).
26. T. Aono and S. Tamura, Phy. Rev. B, **55** (11), 6754 (1997).

Fig.1 : Particle Displacements for a Surface Rayleigh Waves

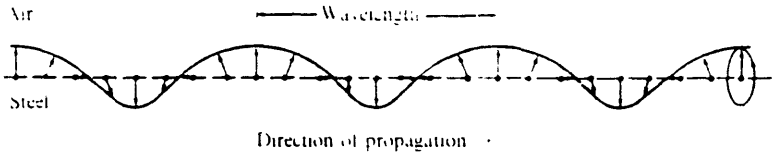

FIGURE 6-2
Particle motion for surface (Rayleigh) waves (*From Krautkramer and Krautkramer [10] Courtesy Springer-Verlag*)

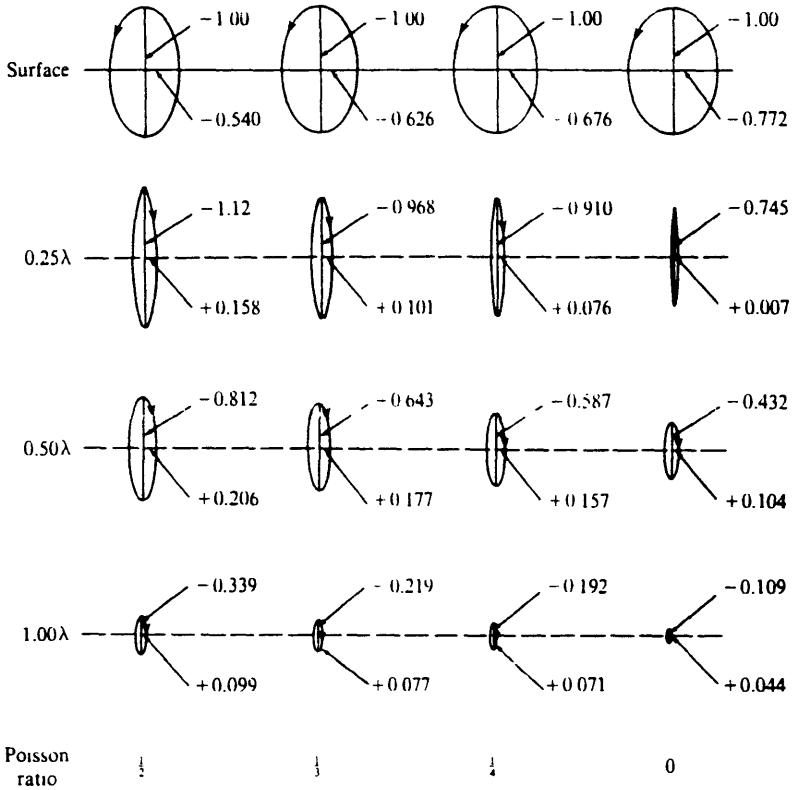

FIGURE 6-4
Particle displacements for a surface wave at various depths below the surface. Note reversal in oscillation direction below the surface. (*From Cook and Van Valkenberg [16] Courtesy American Society of Testing and Materials*)

Fig.2 : Normal Dispersion Curves for Lamb Modes of Rayleigh-type and Love-type

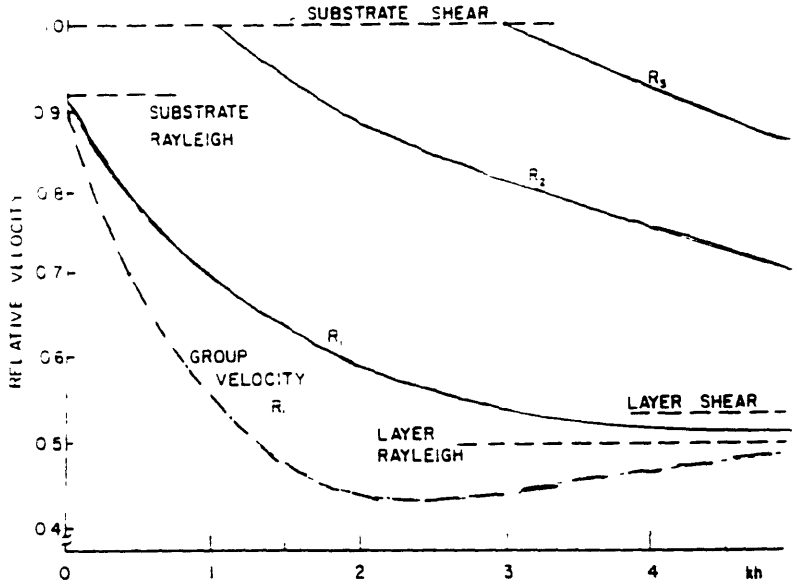

Fig. 2.14 Normalized dispersion curves for Rayleigh modes of a ZnO layer on an isotropic silicon substrate. Broken curve is group velocity of first Rayleigh mode

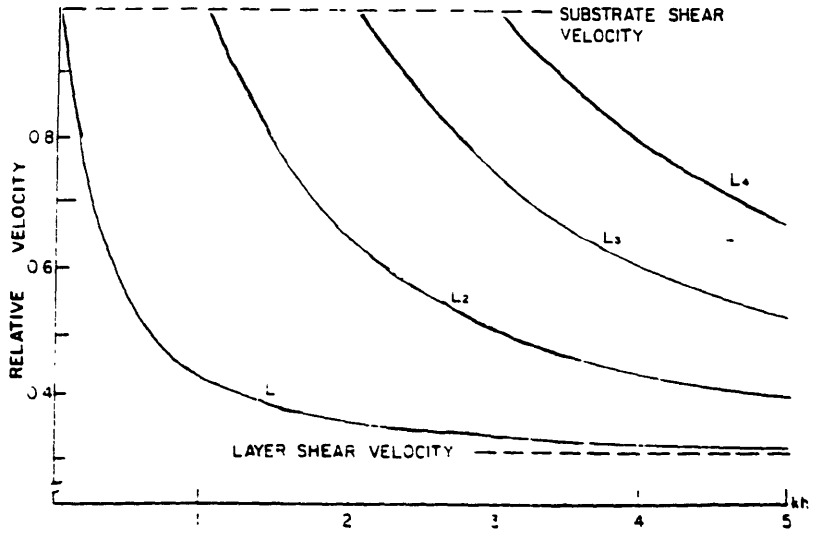

Fig. 2.19 Normalized dispersion curves for the Love modes of a gold layer on a fused quartz substrate

Fig.3 : Schematic of a Reflective-mode Heterodyne Setup for ISTS Experiment

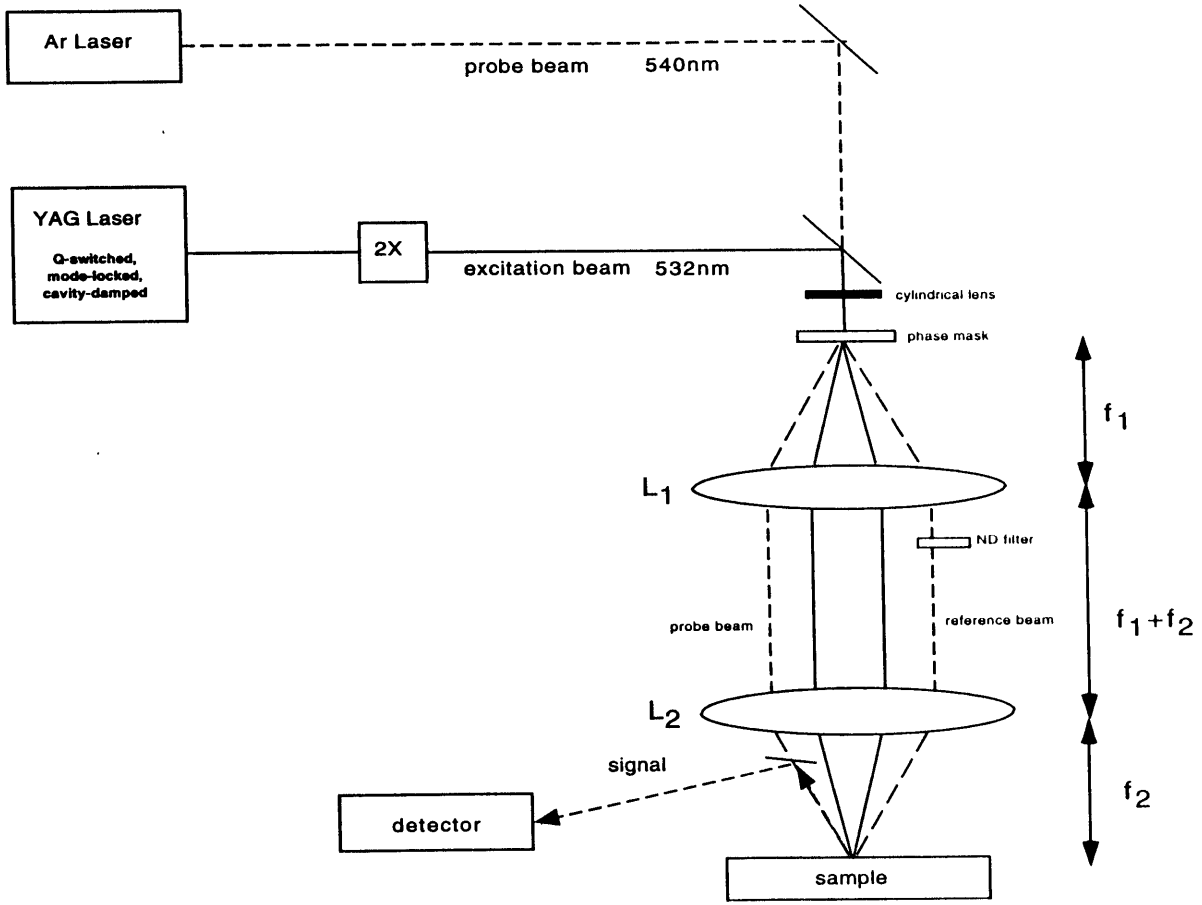

Fig.4 : An Example of Surface Acoustic Response Signal from Ti/Si(001) at [100] Direction for qd=0.45

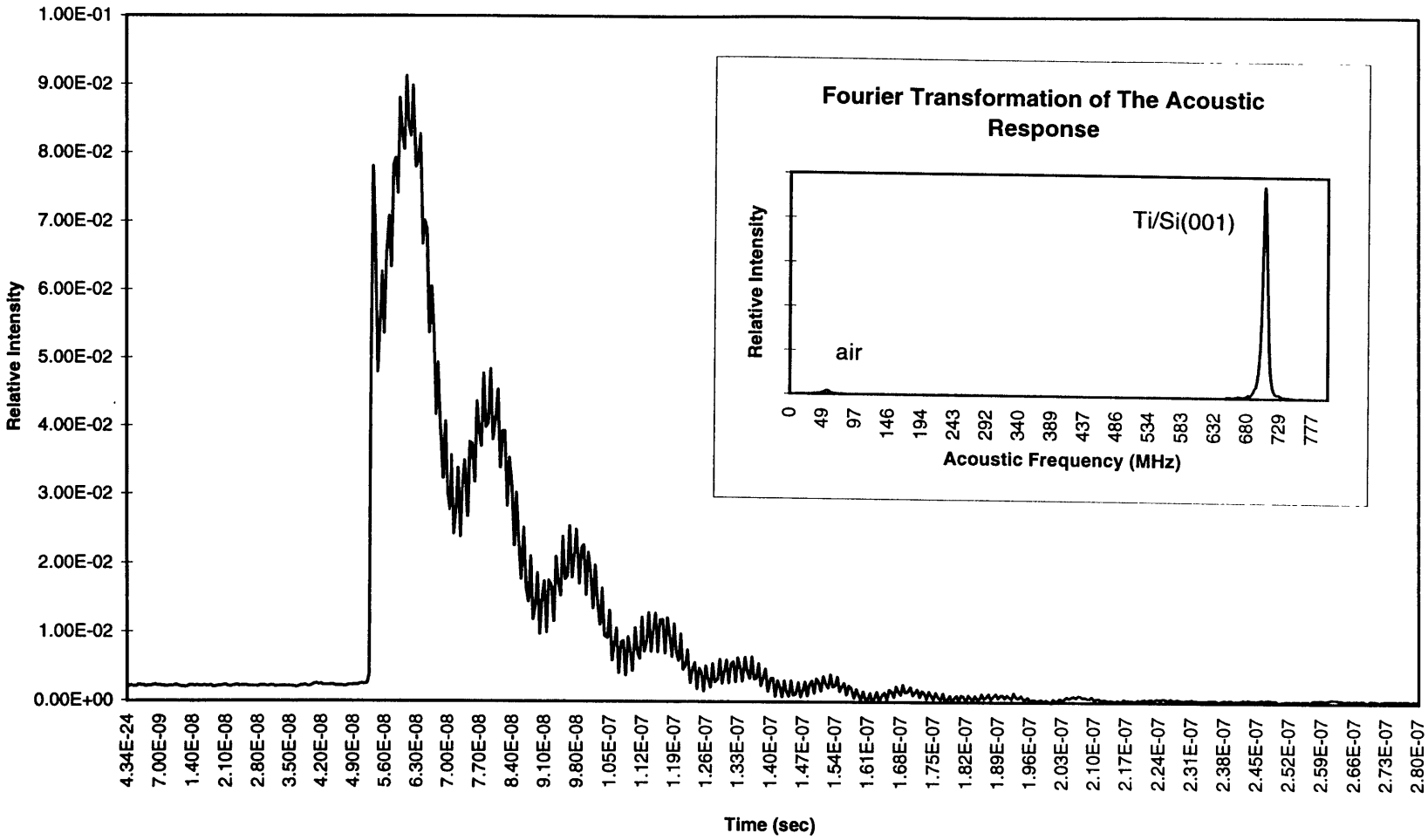

Fig.5 : Angular Dependence of Acoustic Velocities on Ti/Si(001) for qd=0

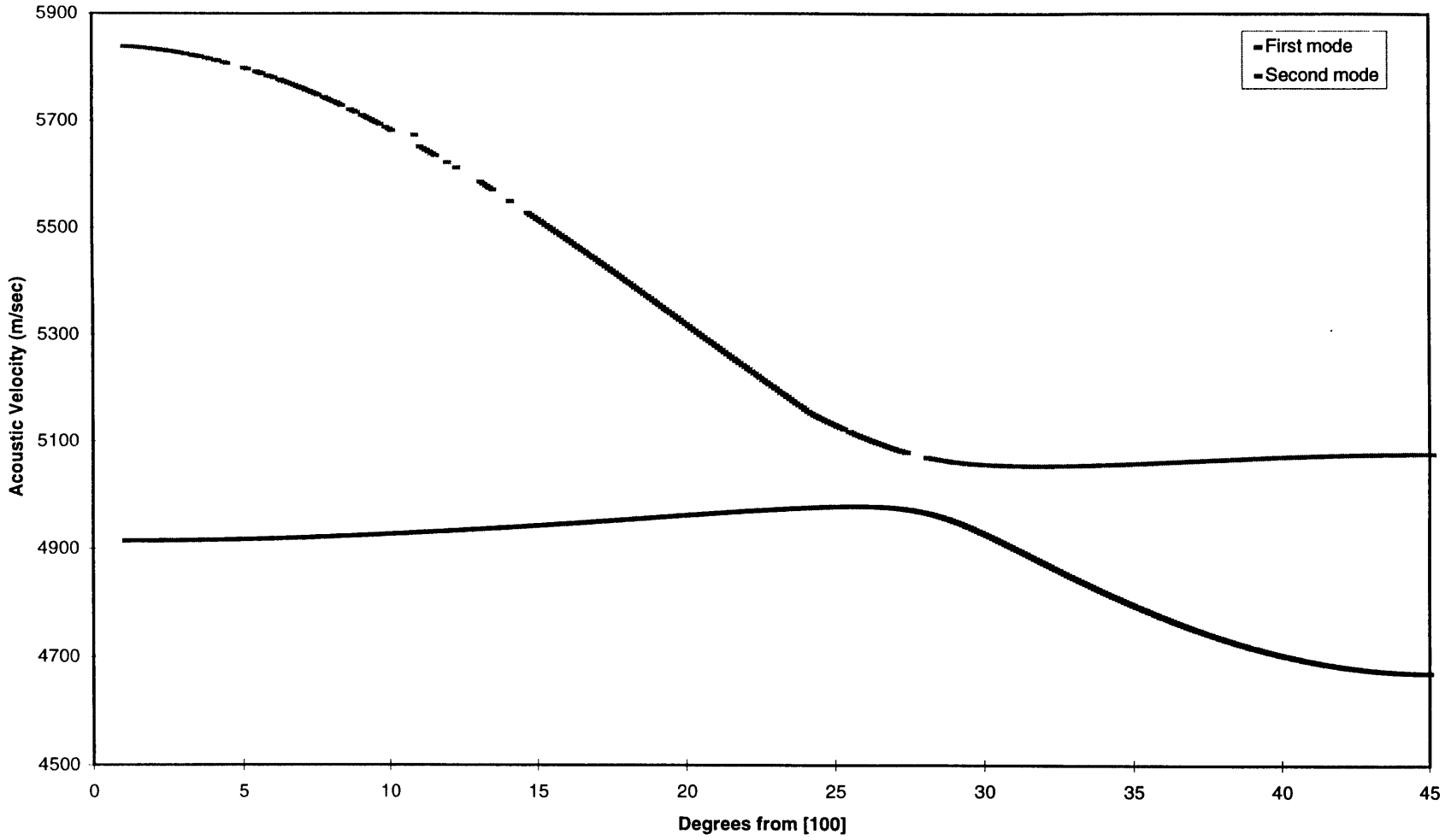

Fig.6 : Angular Dependence of Acoustic Velocities on Ti/Si(001) for qd=0.23

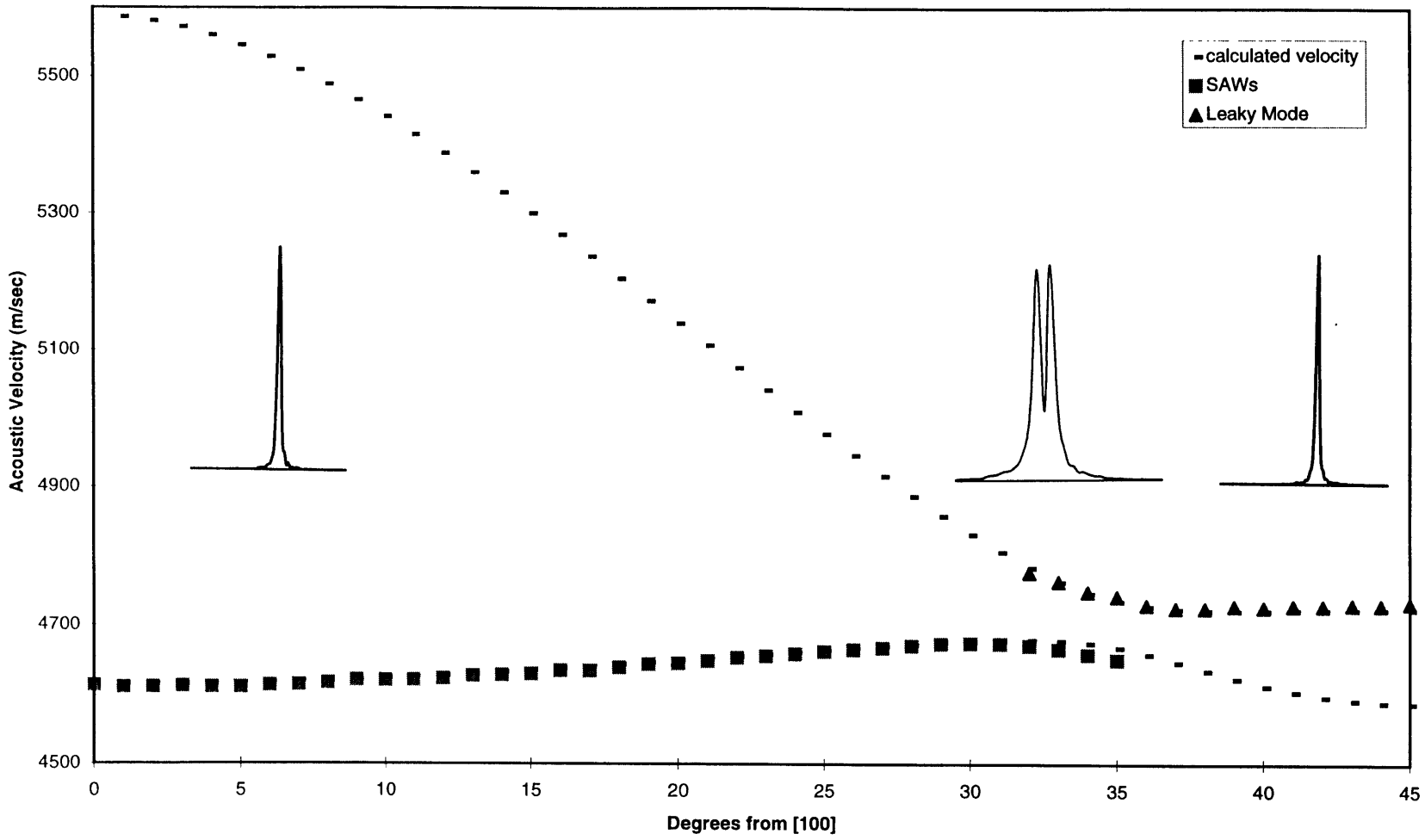

Fig.7 : Angular Dependence of Acoustic Velocities on Ti/Si(001) for qd=0.31

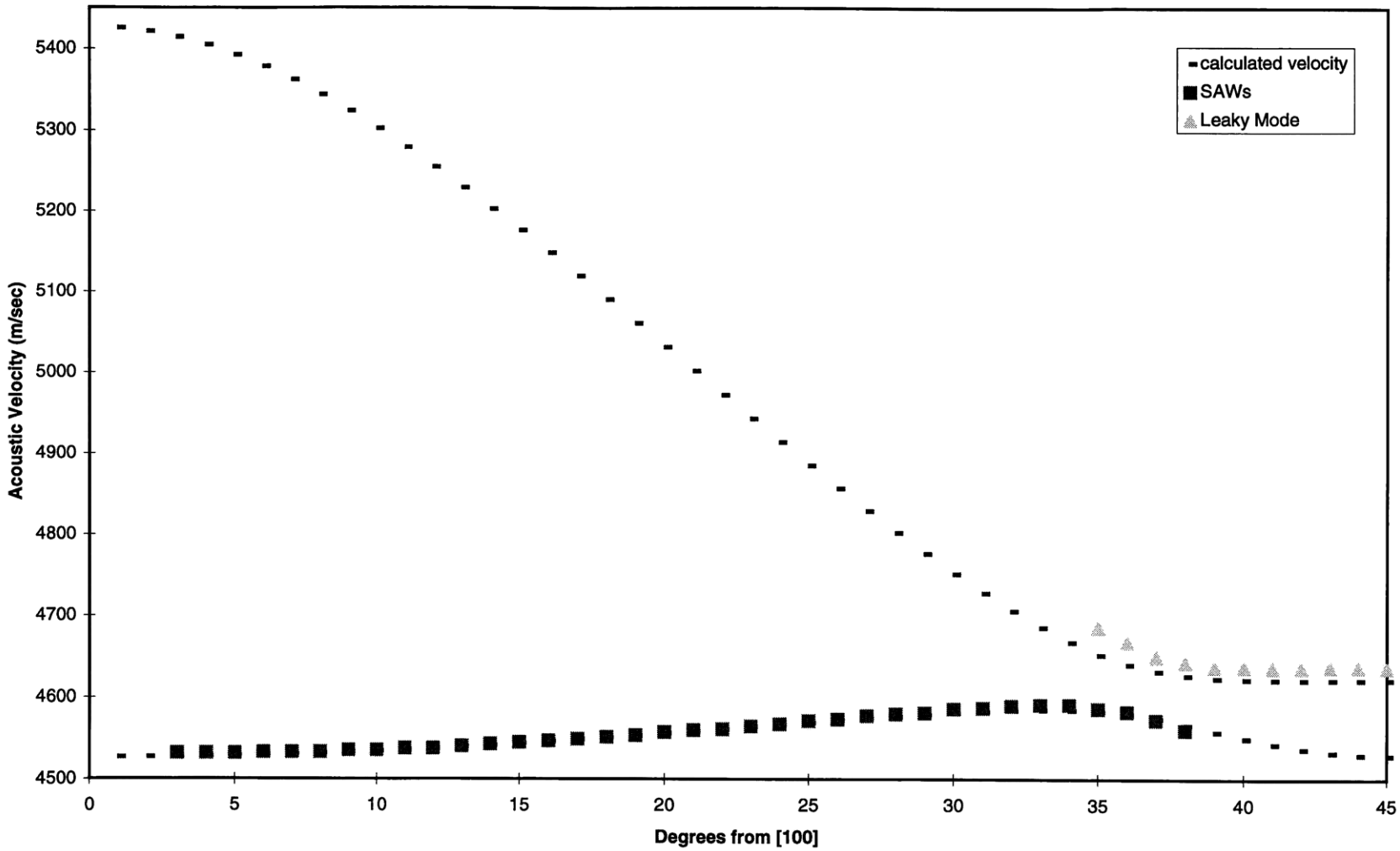

Fig.8 : Angular Dependence of Acoustic Velocities on Ti/Si(001) for qd=0.55

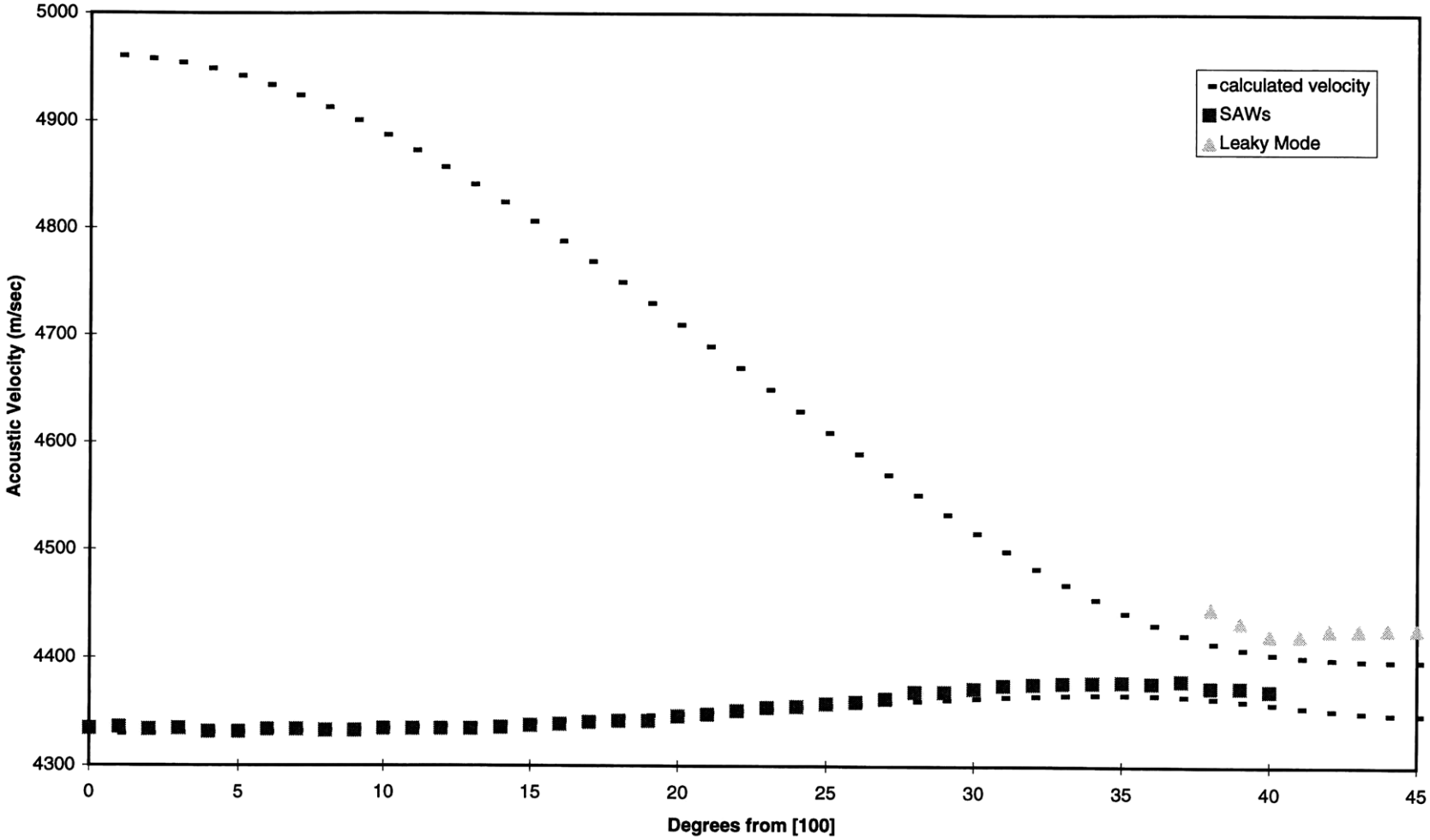

Fig.9 : Angular Dependence of Acoustic Velocities on Ti/Si(001) for qd=0.86

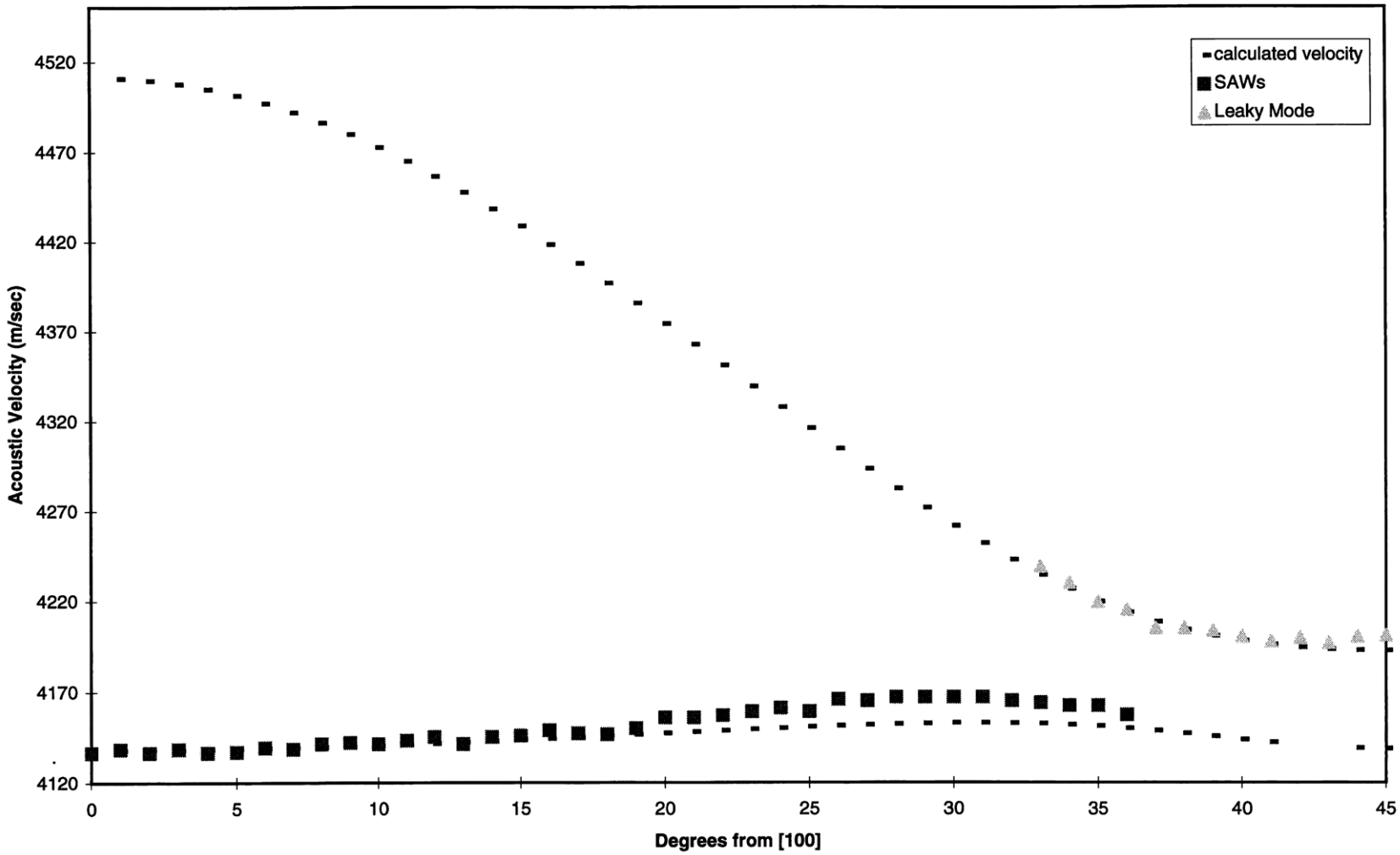

Fig.10 : Fourier Transformed Data Illustrating Two Peaks of Acoustic Velocities

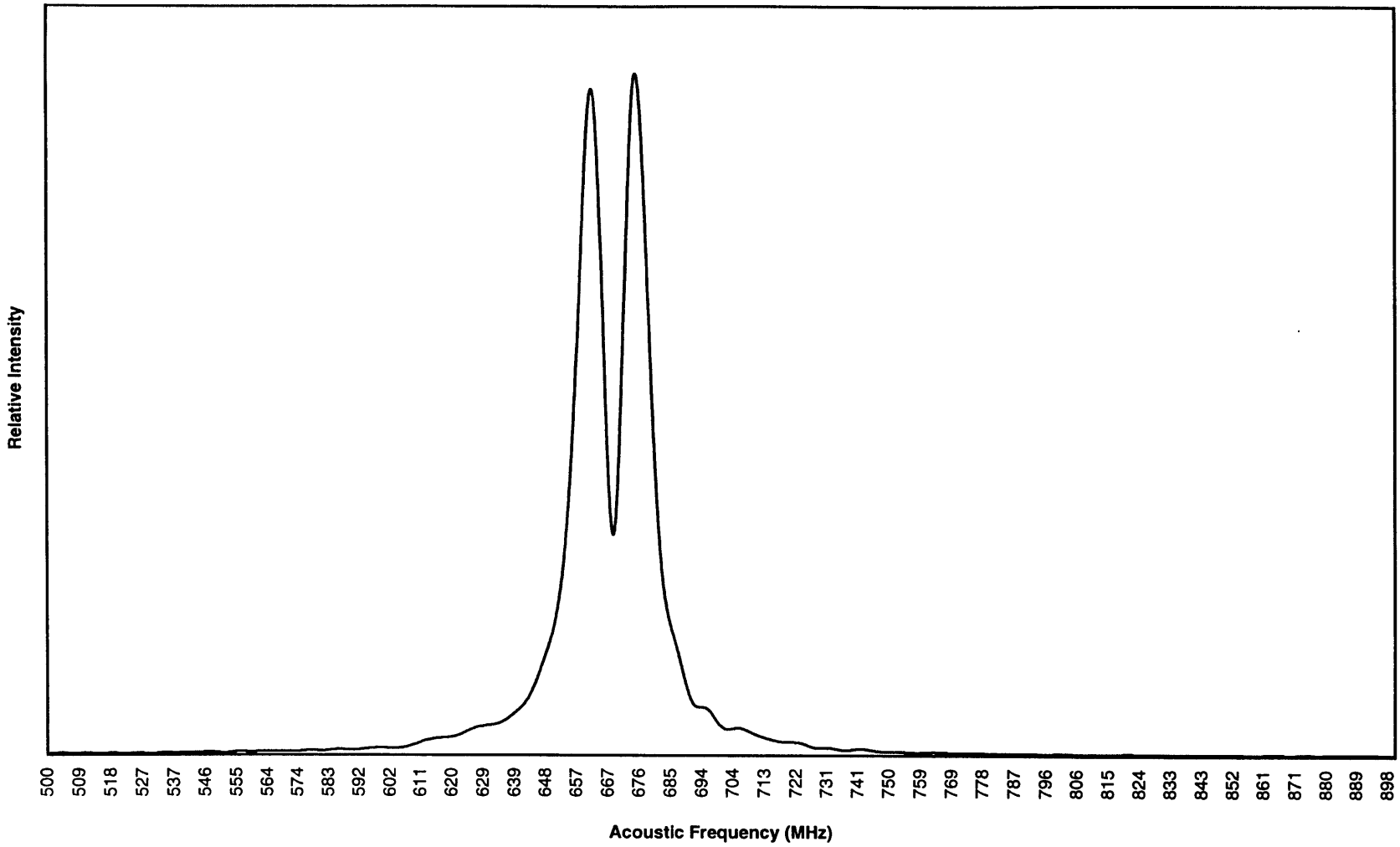

Fig.11 : Dispersion Curve of Ti Film on Si(001) at [100] Direction

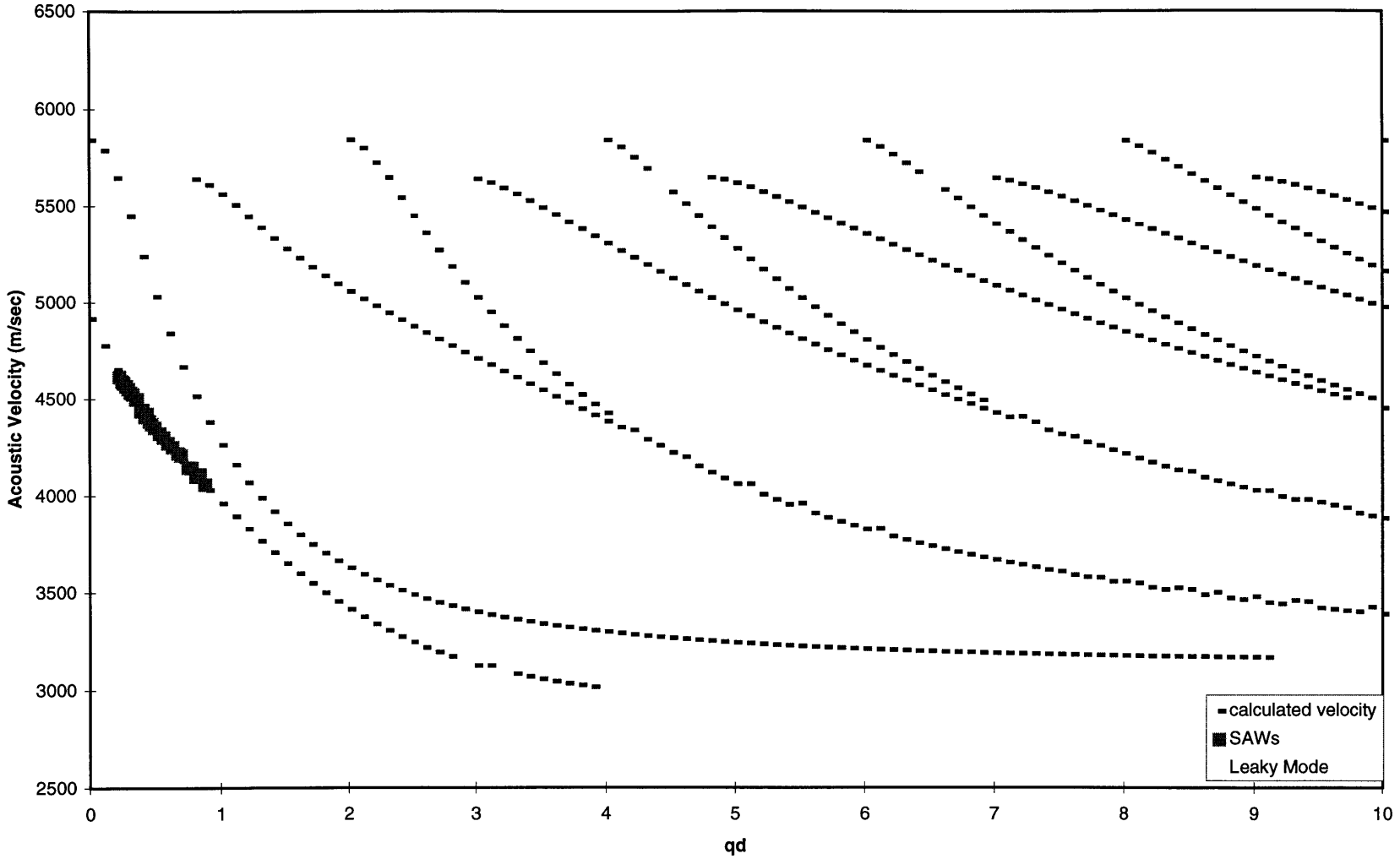

Fig.12 : Dispersion Curve of Ti FIlm on Si(001) at [100] DIrection

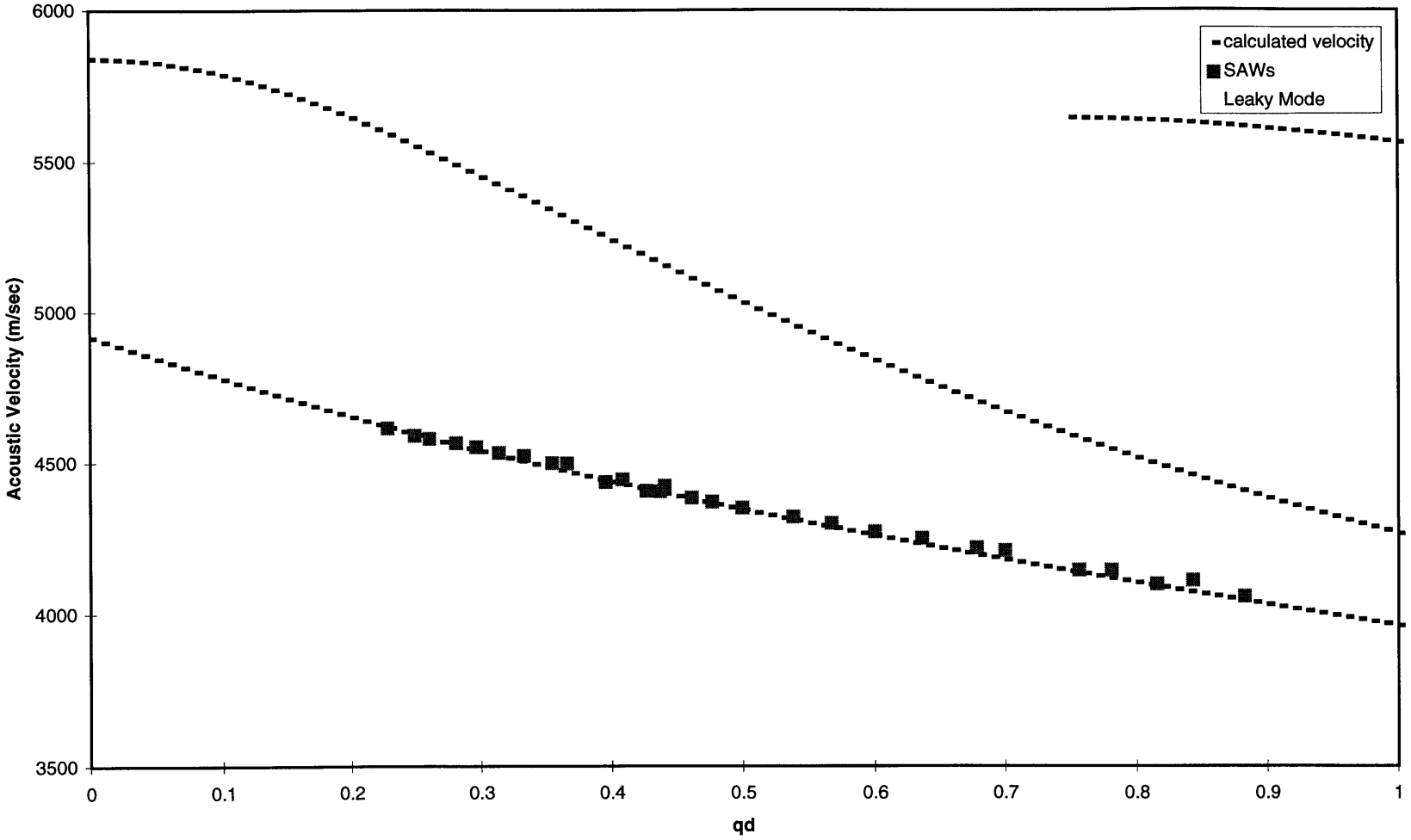

Fig.13 : Dispersion Curve of Ti Film on Si(001) at [110] Direction (45 Degrees from [100])

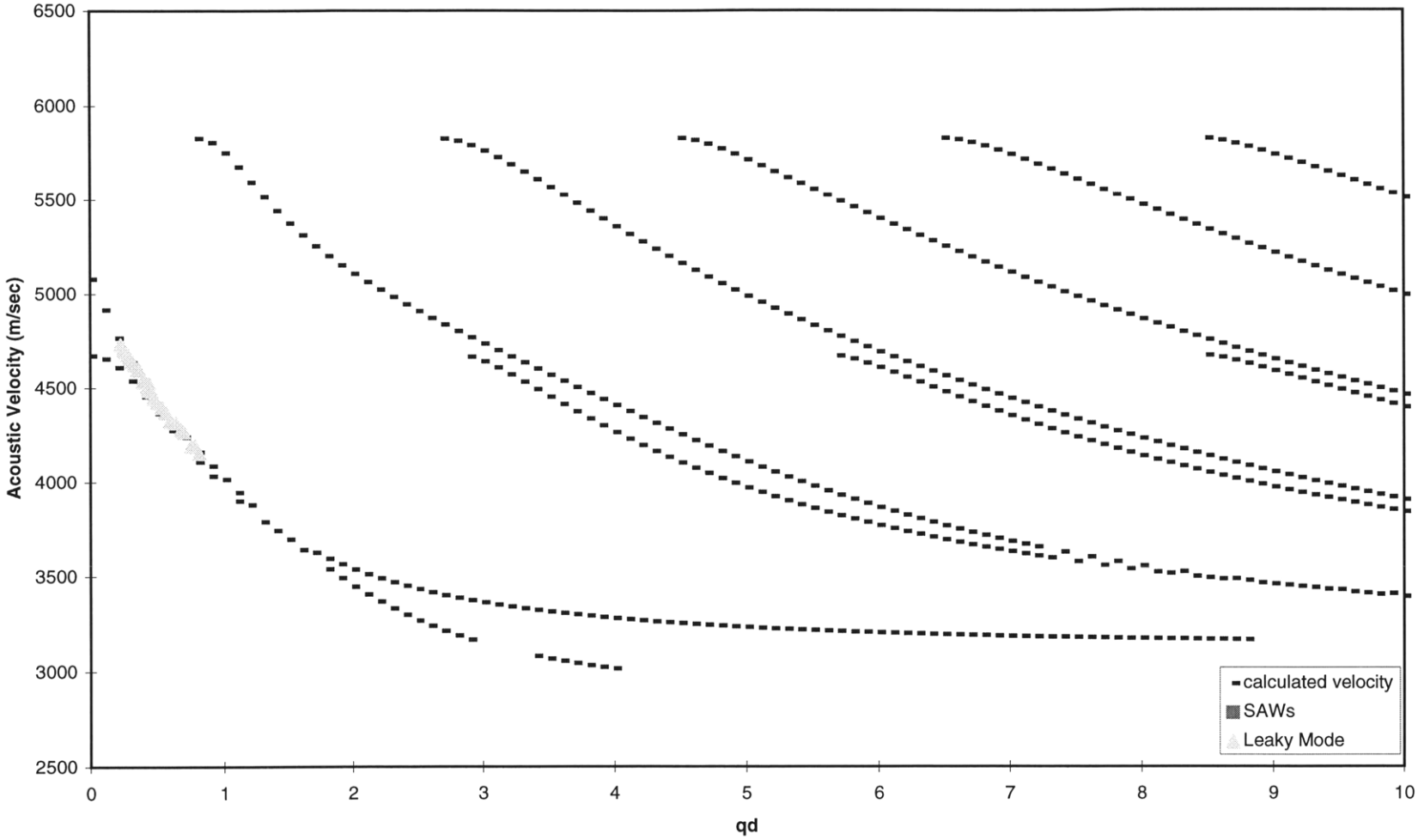

Fig.14 : Dispersion Curve of Ti Film on Si(001) at [110] Direction

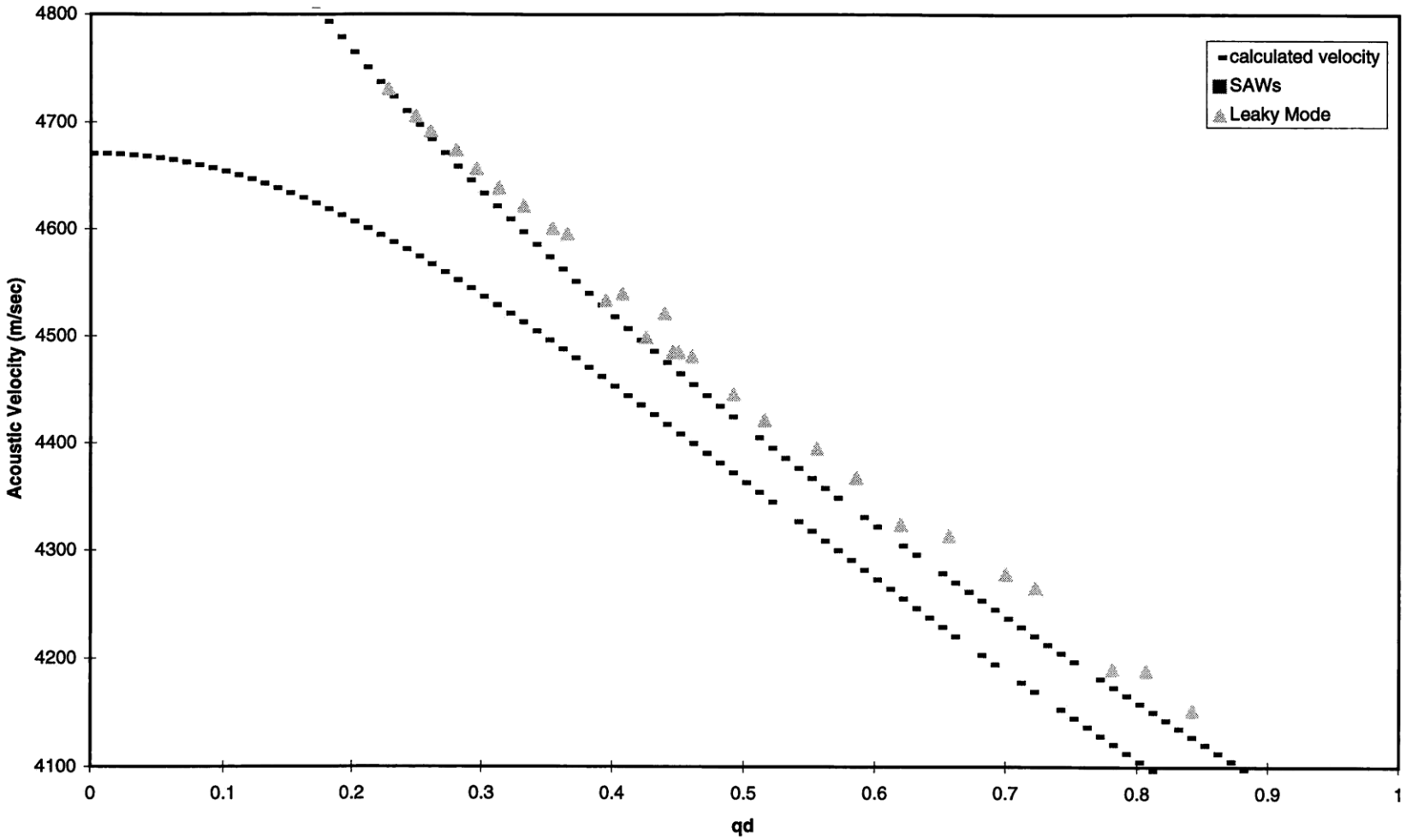

Fig.15 : Angular Dependence of Acoustic Velocities on Ti/Si(111) for qd=0

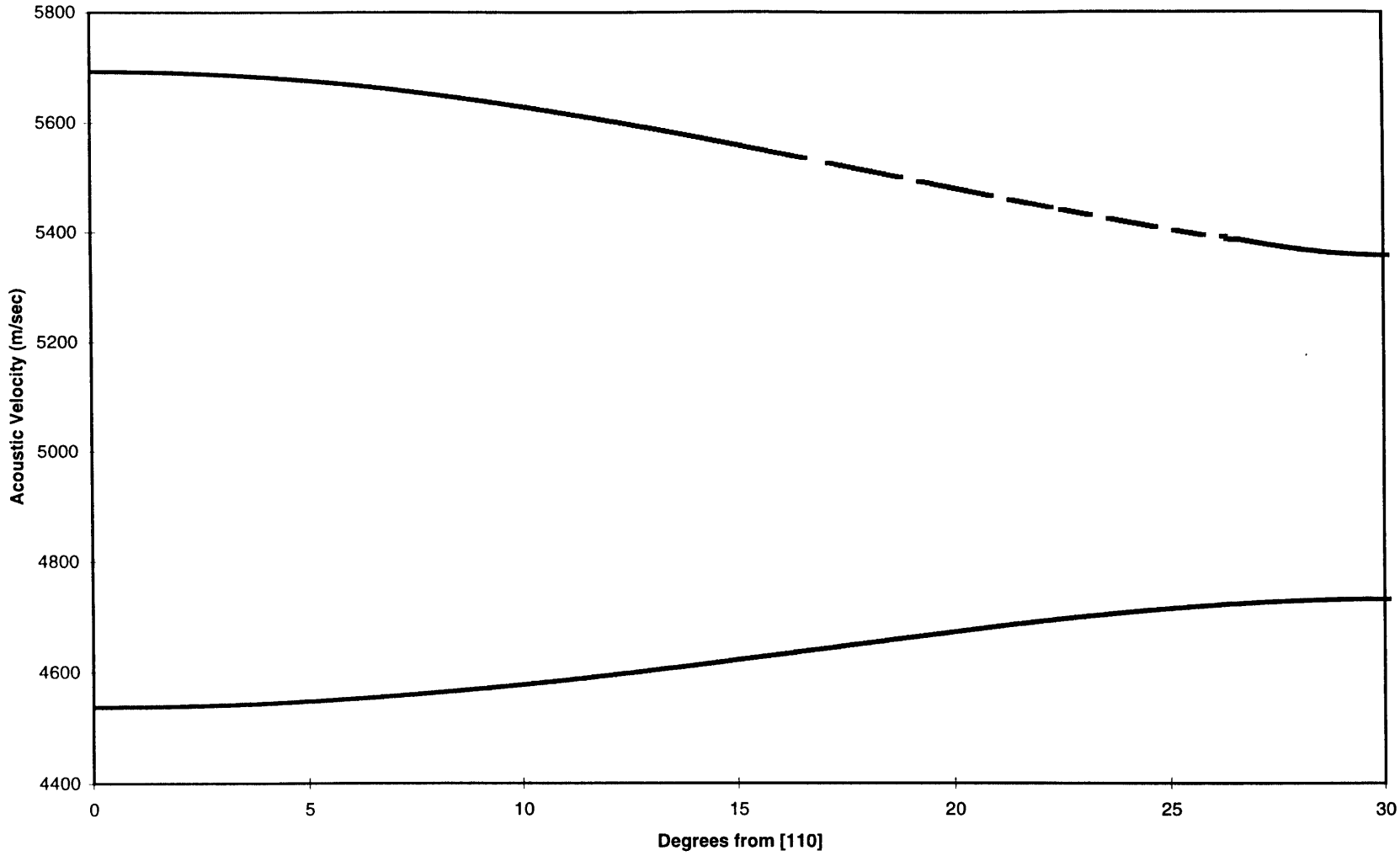

Fig.16 : Angular Dependence of Acoustic Velocities on Ti/Si(111) for qd=0.26

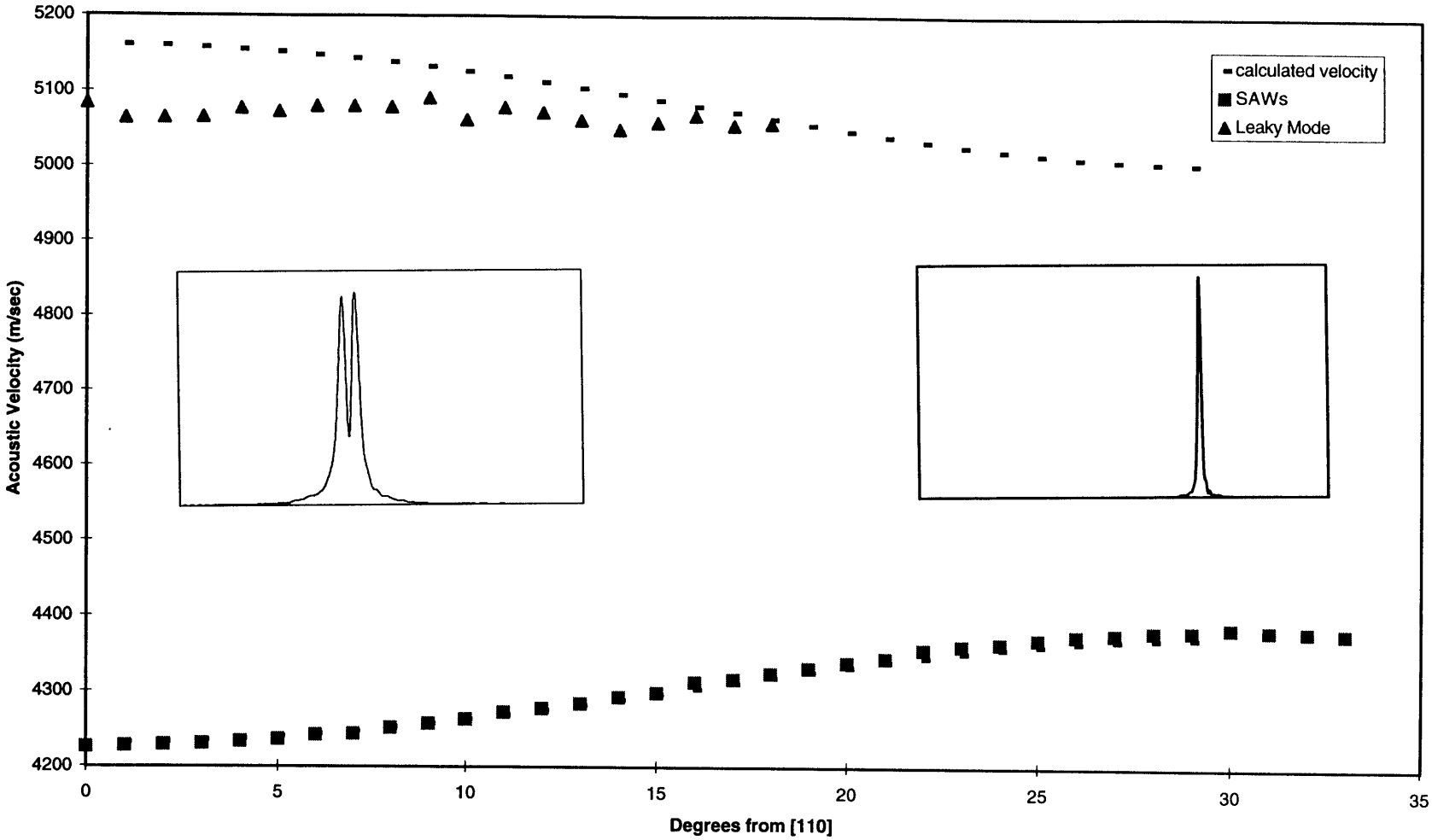

Fig.17 : Angular Dependence of Acoustic Velocities on Ti/Si(111) for qd=0.55

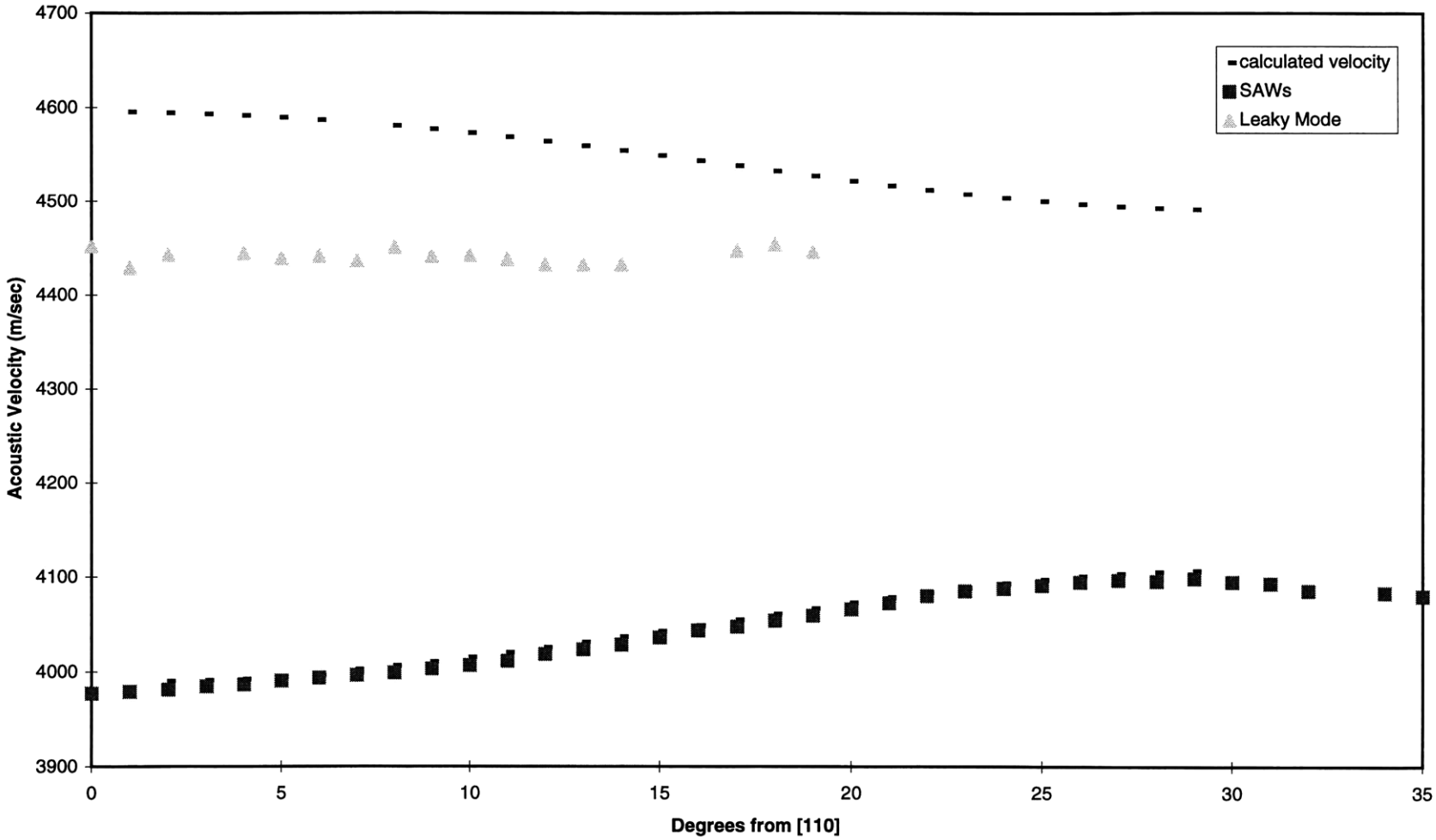

Fig.18 : Dispersion Curve of Ti Film on Si(111) at [110] Direction

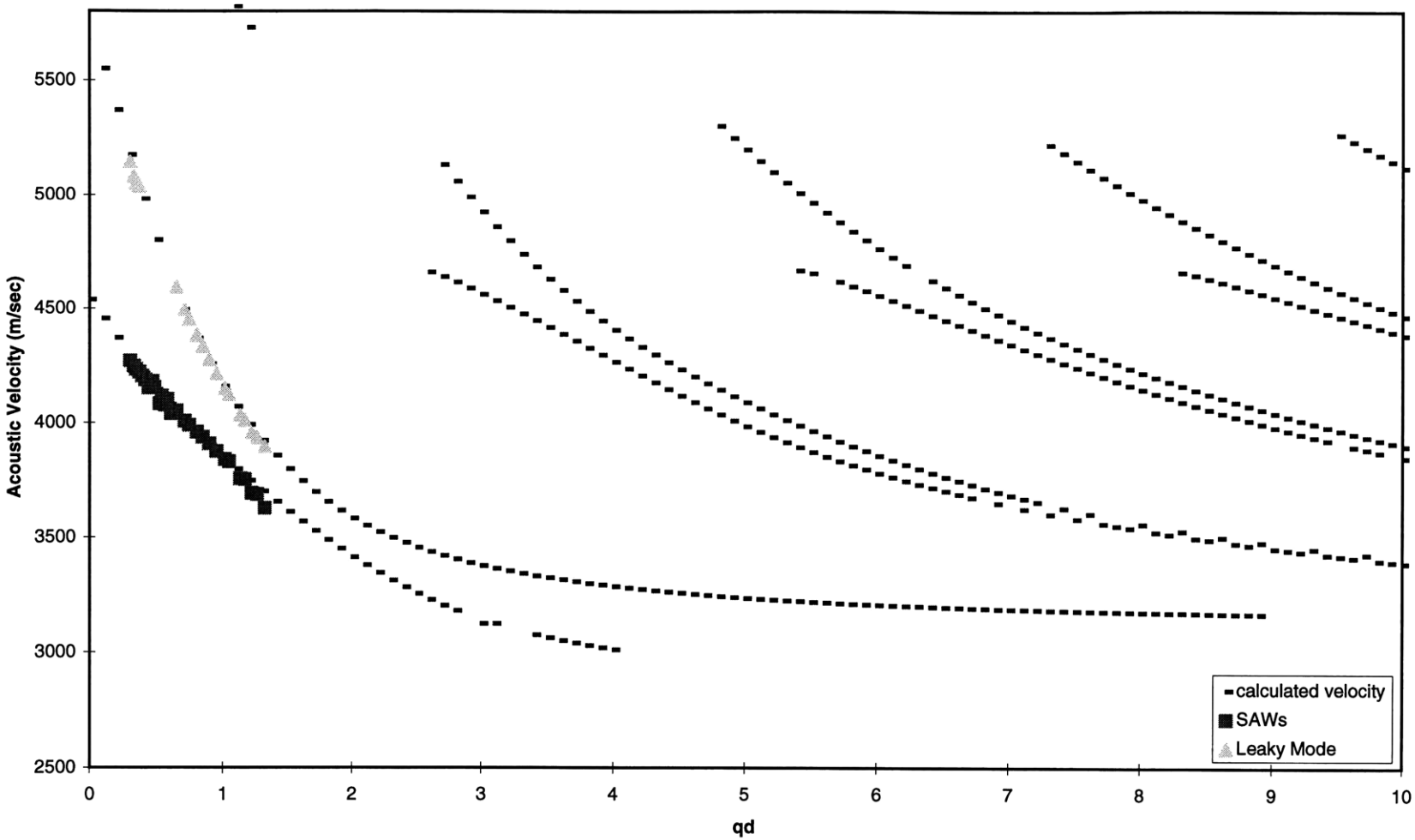

Fig.19 : Dispersion Curve for Ti Film on Si(111) at [110] Direction

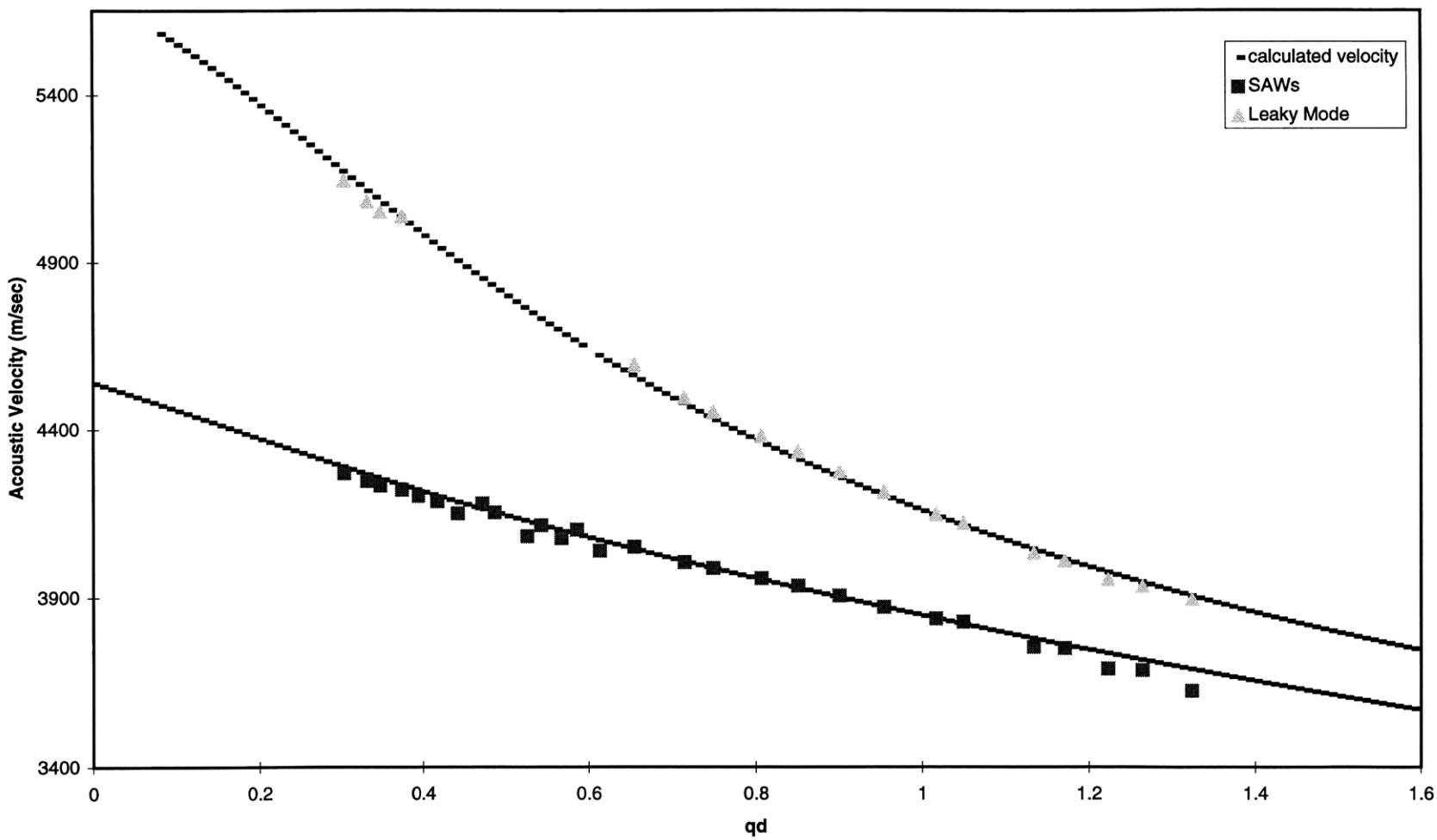

Fig. 20 : Dispersion Curve of Ti Film on Si(111) at [112] Direction

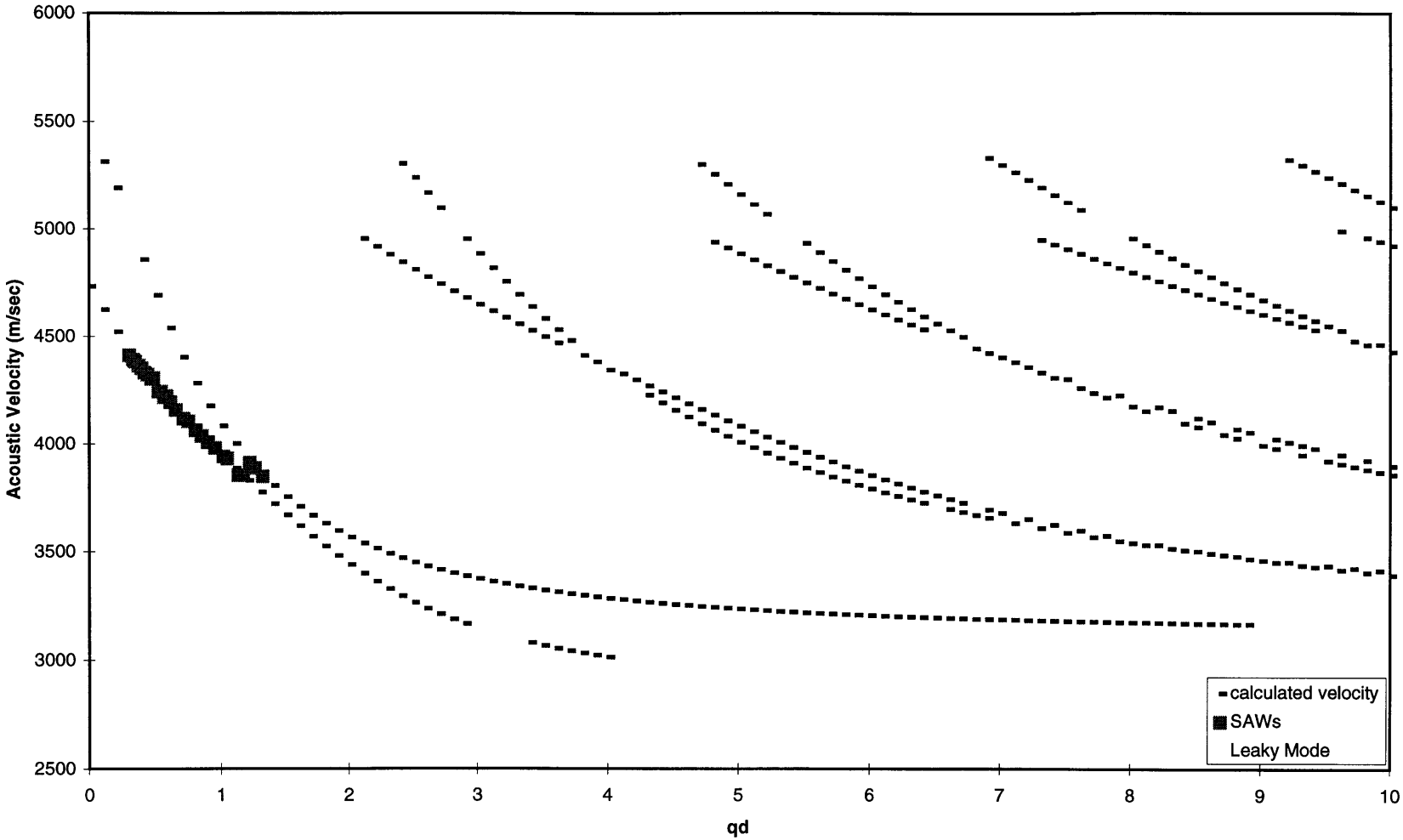

Fig.21 : Dispersion Curve of Ti Film on Si(111) at [112] Direction

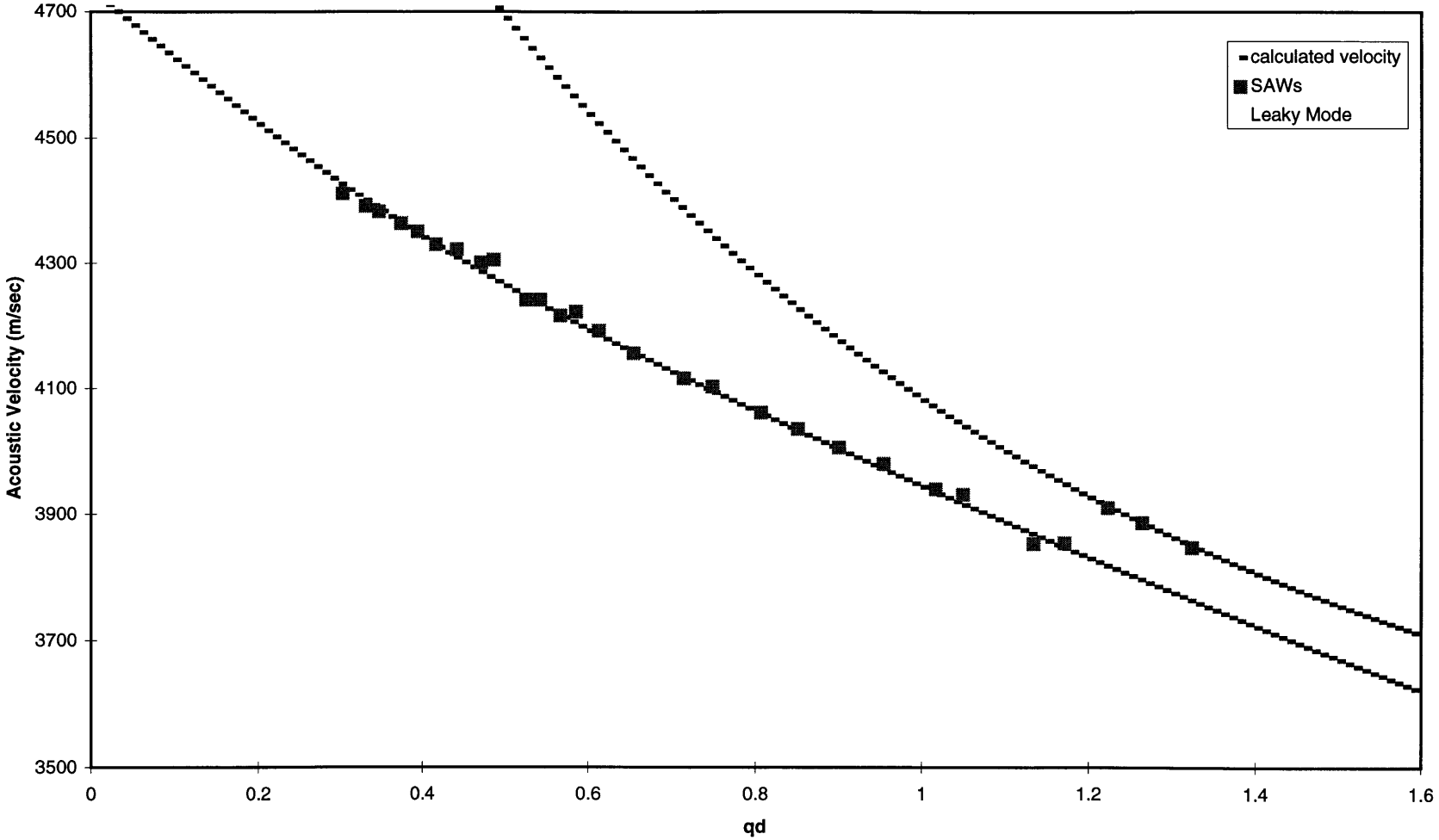

Fig.22 : Dispersion Curve Comparing Isotropic Model to Anisotropic Model of (001) Plane [110] Direction

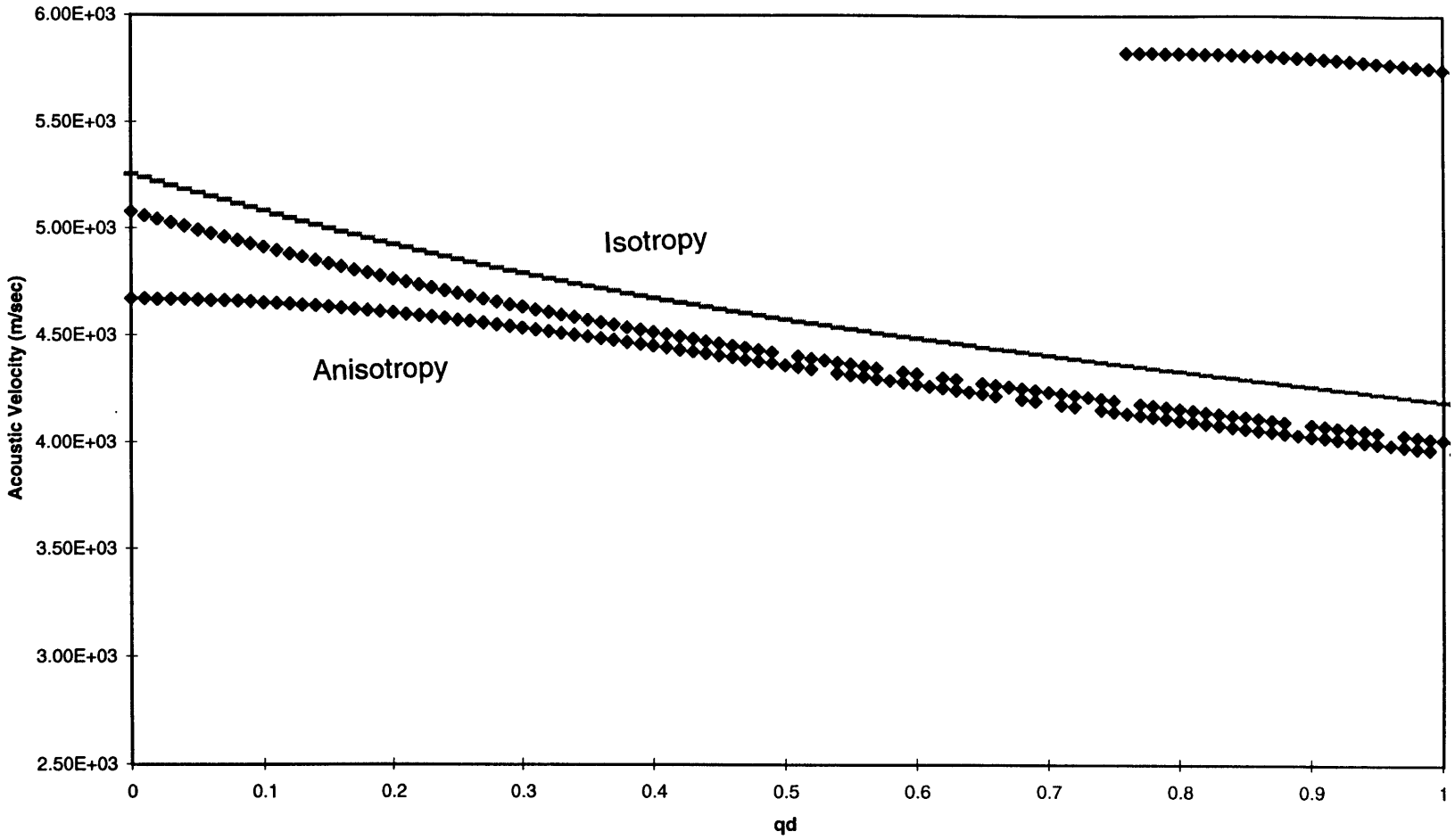

Fig.23 : Acoustic Responses From Damascene Structure of 75% Specific Density of Copper with Different Bar Widths

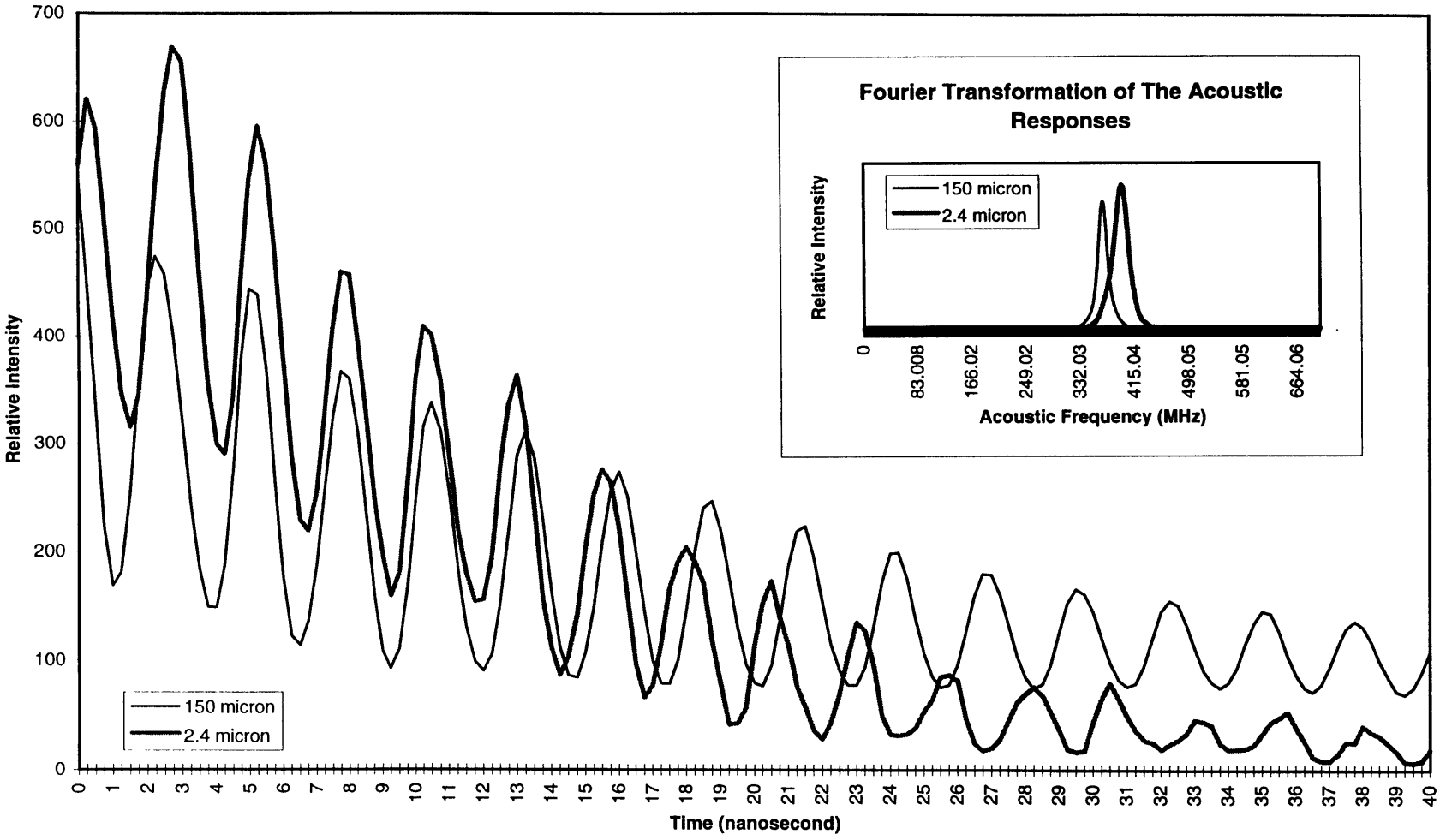

Fig.24 : Acoustic Responses From Damascene Structure of 66.67% Specific Density of Copper with Different Bar Widths

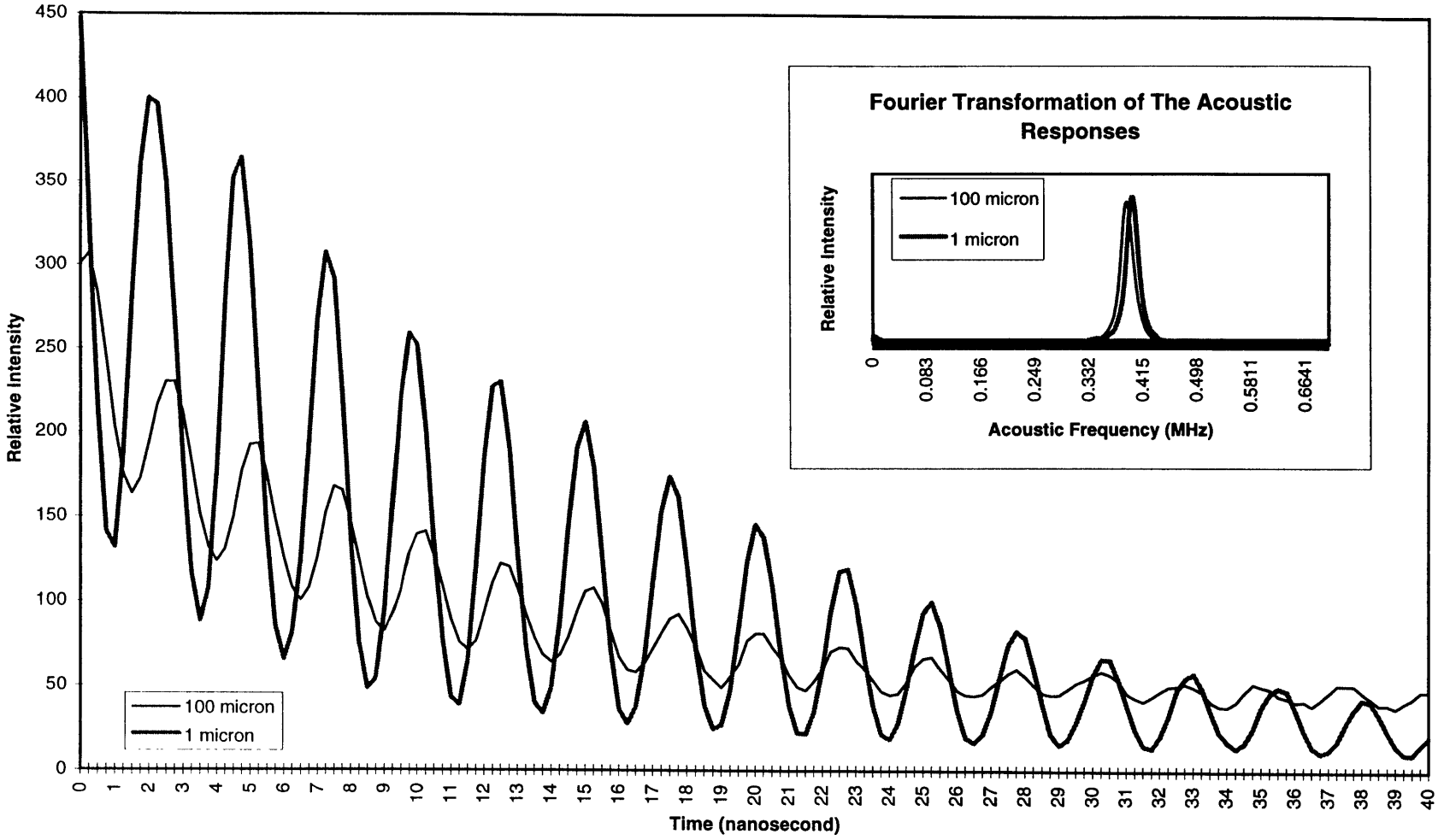

Fig.25 : Acoustic Responses From Damascene Structure of 3 Micron Bar Width

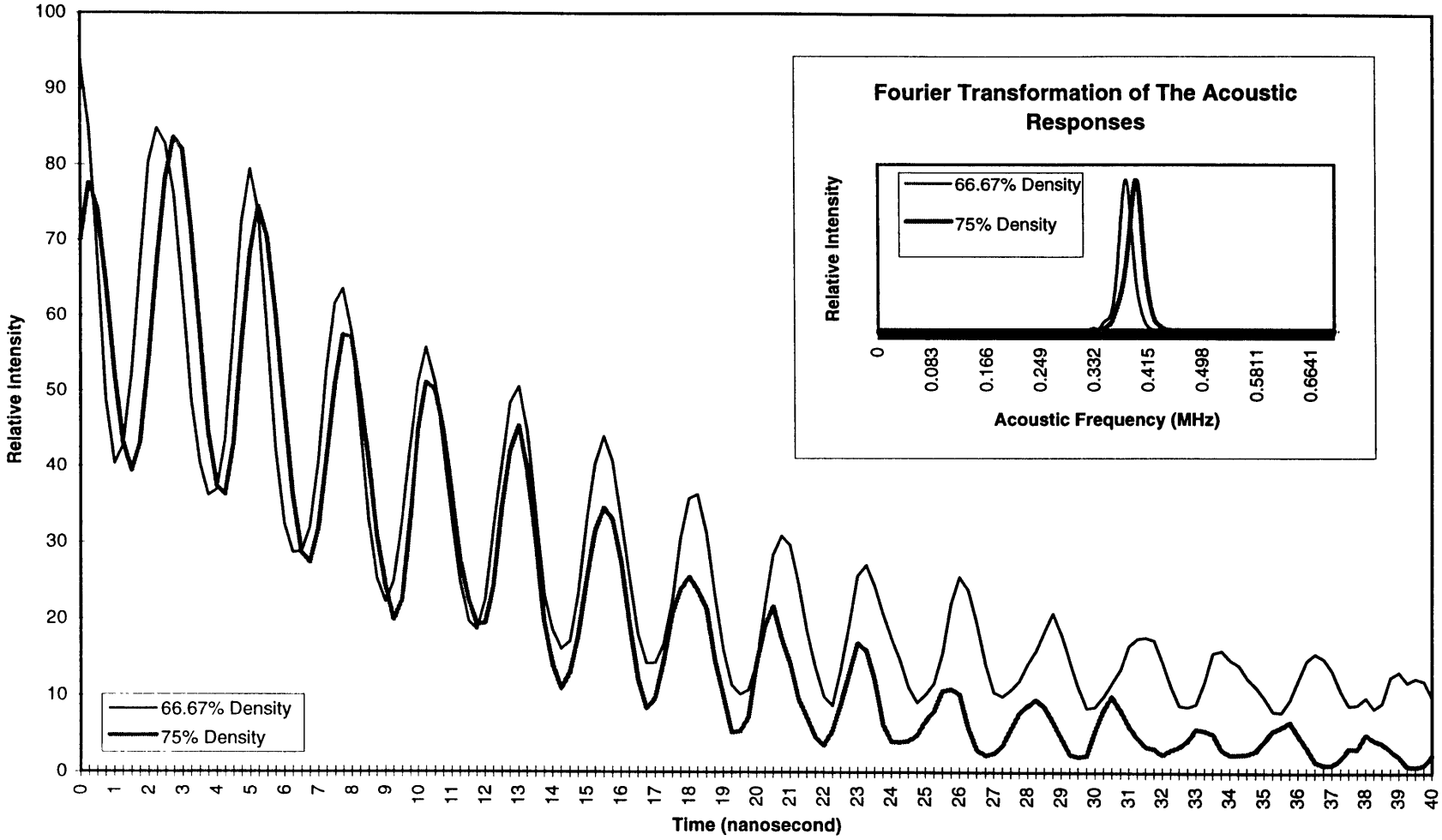

Fig.26 : Acoustic Responses From Damascene Structure of 2 Micron Bar Width